Comparison Between the Bath and the 4D 6000 Instantaneously Phase Shifted Interferometers

3rd Year Dissertation

Maxwell L. Edwards

Astrophysics BSc, Institute of Mathematics, Physics and Computer Science,
University of Aberystwyth

Abstract

Recent research has suggested that Bath interferometer technology has the capability of being a highly accurate, low cost optical measuring instrument. In order to investigate these reports, the following experiment was conducted which compares the Bath interferometer to the industry leading 4D Technology "dynamic" PhaseCam 6000 laser interferometer (4D PhaseCam). The two interferometers were used to obtain surface readings of two dissimilar spherical mirrors and the results then compared. The Bath interferometer proved to be consistently accurate by producing RMS readings of each optic that were just 2.94 ±2.22 nm (of a optic with a surface RMS of 117.05 ±2.22 nm) and 0.21 ±0.92 nm (of a optic with a surface RMS of 16.85 ±0.92nm) different from the result obtained by the 4D PhaseCam. Considering the Bath prototype built for this experiment has a construction cost of around £120 - one thousand times less than the market price of the 4D PhaseCam - recent reports that the Bath interferometer is extremely precise have been supported by this investigation.

Table of Contents

Acknowledgements

The author would like to take the opportunity to thank David Thomson at Glyndwr Innovations for his major contribution to the project. Without his lead in the construction of the Bath interferometer prototype and insight into the technology, this investigation would not have been possible.

Also, to Kayleigh Thomson for her aid and direction of the project. Without her knowledge of the field and organisation, the project would not have progressed in the manner that it did. To Professor Paul Rees of OpTIC Glyndwr, for his guidance into how to efficiently analyse the results. The author also thanks his supervisor Dr. Martin Wilding and his colleague Martin Lee.

The author would also like to extend his thanks to Dale Eason for making OpenFringe freely available and for his research conducted into the Bath interferometer.

Finally, the author would like to extend his thanks to the authors of the referenced literature for making their research accessible.

1. Introduction to Science

This section will include an introduction into the base science of the project along with some necessary information required to understanding the project.

1.1 Experimental Purpose

As discussed in the literature review, the goal of the project is to investigate the optical design of two different interferometers and construct a prototype that can fill the void in the market for a low cost, reliable, high precision interferometer. This would provide optical polishers with the opportunity of obtaining precise and reliable surface readings for minimal cost, or allow amateur astronomers to test their optics for irregularities that might be affecting image quality. The Bath interferometer design was selected due to its versatility, simplicity and its reported potential accuracy **[1]**. As this design has seen limited documented use, the purpose of this experiment was to determine an absolute precision of the Bath interferometer and identify any possible limitations it might contain such as its sensitivity to environmental factors. Initial tests were conducted on its accuracy and its sensitivity to thermal air currents using multiple optical parts. Once readings had been obtained with the Bath interferometer, the results were compared to readings obtained from the industry's leading technology, the 4D Technology PhaseCam 6000 dynamic laser interferometer (4D PhaseCam) **[2]**. The latest quote for the 4D PhaseCam is £140,000, meaning it is over 1000 times more expensive than the Bath prototype. The comparison conducted in this report has provided insight into the capabilities of the Bath interferometer and in turn determine if it is a technology worth pursuing.

1.2 Introduction to Interference of light & Interferometry

Interferometry utilises the principle of superposition of waves that states that when two (or more) waves travelling through the same medium at the same time, the net displacement of the medium at any point in space or time, is simply the sum of the individual wave displacements **[3]**. With the right instruments and set up, meaningful information can be extracted from the superposition of waves **[3]**. This can be achieved in multiple ways and over the years many different techniques and experiments have been developed to extract information from the interference of waves. Experiments such as the Michelson-Morley **[4]** and Young's double-slit **[5]** experiments have gone down in history as a couple of the most important experiments to date due to their monumental significances, with both utilising the concept of light interference.

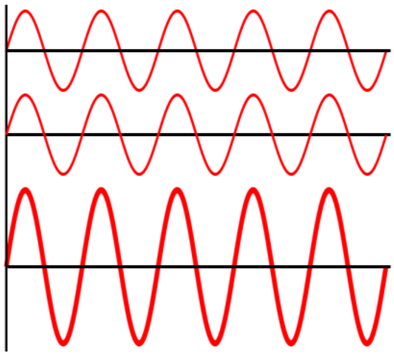

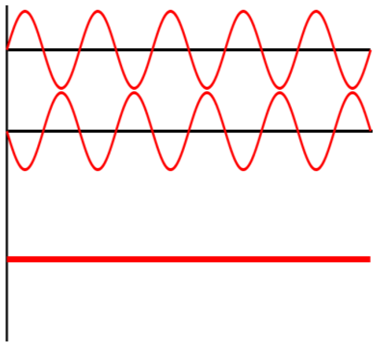

Figure 1: Examples of two waves traveling in phase and the resultant wave when the waves superimpose.

Figure 2: Examples of two waves traveling 180^{o} out of phase and the resultant wave when the waves superimpose.

Interferometers work by implementing the use of 2 beams of light, one traveling to the surface to be measured (part under test), the other to a reference surface. The light beams then return and superimpose onto a surface causing an interference pattern representing the surface of the part under test, known as an interferogram (Figure 3). If the surface of the part under test is perfectly spherical, the two light beams will construct destructively causing the interference pattern to represent a flat surface. But if the test piece is irregular, the interference pattern will contain the information of where these irregularities lie, and once analysed can be visually represented (Figure 4). Due to the laser having a wavelength of light, any small surface irregularity will cause a large change in the phase of the wave. This means that surface irregularities down to the nano meter can be identified through the interference of the test and reference light beams. Clearly the reference surface needs to be near perfect, otherwise it would cause phase changes in the reference beam leading to false readings of the test piece.

Interferograms are vital as they allow one to visualise a surface to extremely small precision. Figure 3 might not appear like much but the pattern displayed is carrying a lot of potential information about the test piece if analysed correctly.

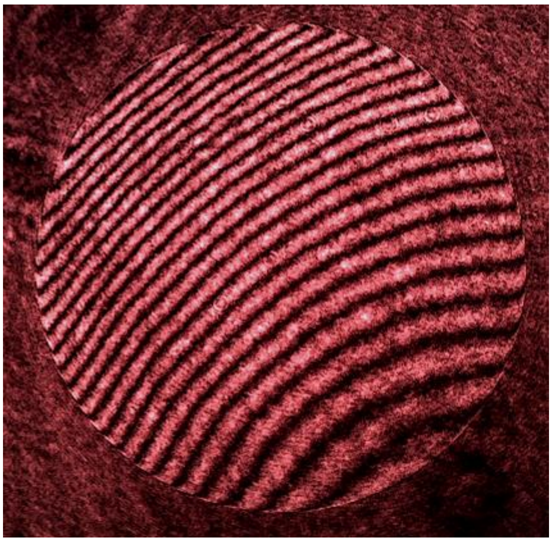

Figure 3: Interferogram produced from a Bath Interferometer captured by a webcam.

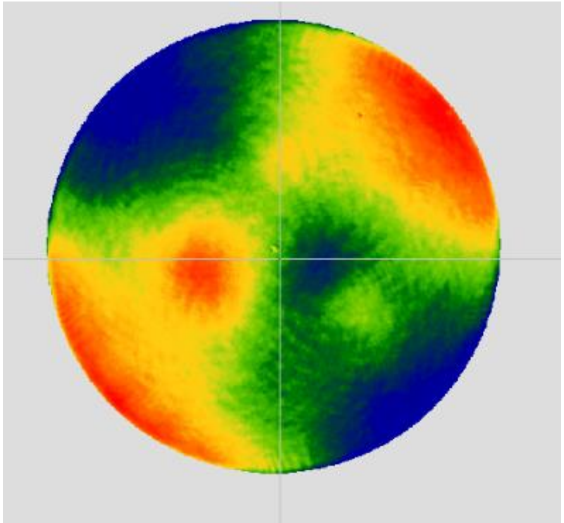

Figure 4: Surface of the test optic produced in the software 4Sight by analysis of the interferogram from Figure 3.

The surface map of the test piece shown in Figure 4 displays the 'flatness' of the surface; red being the elevated regions and blue representing the depressed regions in relation to a perfect surface form. In the Figure 4, the most elevated region is only 200 nanometres above the zero plane, demonstrating the possible precision of interferometer technology.

1.3 Aberration Theory

Understanding aberrations is vital in optical metrology as its principal purpose is to determine the aberrations present in an optical component or an optical system **[6]**. The two types of Wavefront aberrations are monochromatic (Seidel and wave) and chromatic (Longitudinal, Transverse) aberrations. Chromatic aberration is a type of distortion in which there is a failure of a lens to focus all colours to the same convergence point. This occurs because lens's have different refractive indices for different wavelengths of light. With regards to monochromatic aberrations, there are five primary types of Seidel aberrations, these being Spherical aberration, Coma, Astigmatism, Field curvature and Distortion each with their own unique properties (Figure of Seidel aberrations)

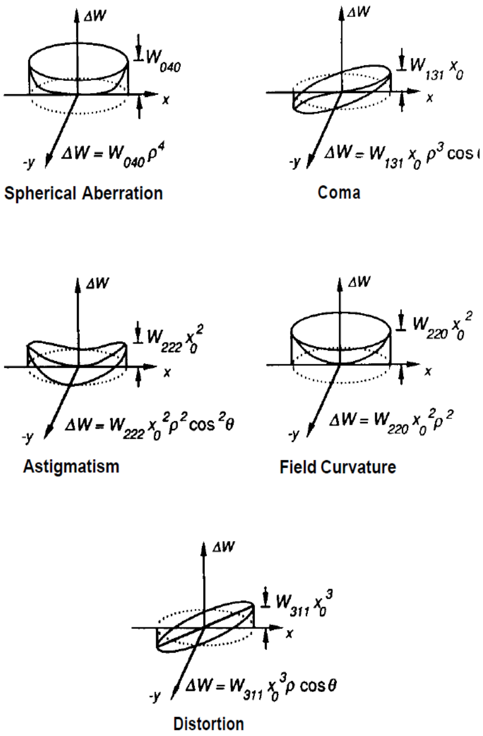

Figure 5: Seidel Aberrations. **[6]**

1.4 Zernike Polynomials

Zernike polynomials are the standard way of modelling aberrations of a surface **[6]**. They are a complete set of orthogonal polynomials across the unit circle, and with the use of coefficients the polynomials can be used to describe the surface of almost any optical surface.

$$W(\_,\theta) = \sum C_n^m \, Z_n^m(\_,\theta)$$

Wavefront aberration

Zernike coefficient

Zernike polynomials (wavefront mode)

Figure 6: Zernike wavefront aberration equation. **[6]**

Figure 6 displays how a wavefront is represented by a sum of Zernike polynomials, each with its own coefficient. Although Zernike polynomials are primarily used for spherical surfaces they can be adjusted to work for a range of different shaped optical surfaces. However, this method has proved to be far inferior. There are an infinite amount of Zernike polynomials, but almost any spherical surface can be accurately represented with the use of around 40 of these polynomials. There are also different orders of Zernike polynomials, each being orthogonal to every other. A few of these polynomials are shown in Figures 7 & 8.

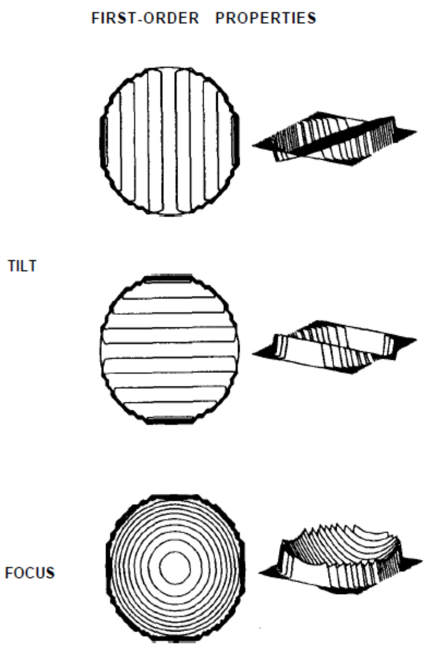

Figure 7: Examples of First order Zernike Polynomials. [6]

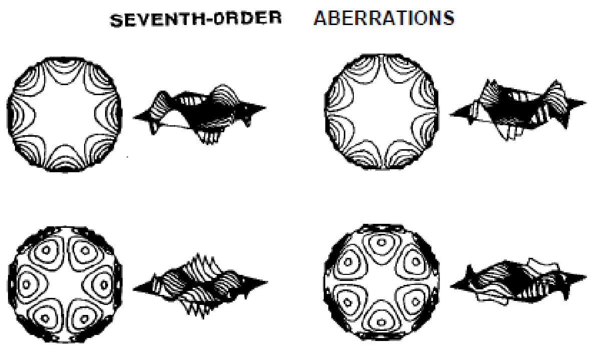

Figure 8: Examples of Seventh-order Zernike Polynomials. [6]

1.5 Environmental Effects

When taking measurements with an interferometer, the surrounding environmental conditions such as temperature, vibration levels and thermal air currents can all lead to large fluctuations in the readings. Environmental conditions are an important factor to consider but can be mitigated through difference procedures of multiple complexities, such as taking multiple frames and then taking the average of the test piece or undertaking long and short statistical analysis.

Vibrations can originate from multitude sources, such as the air conditioning system running a building or just the small vibration of footsteps from a person walking across the room. Whatever the source, vibrational waves cause large irregularities in the readings as represented by Figure 10.

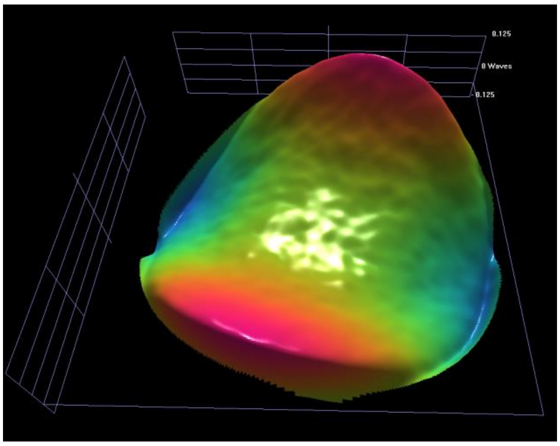

Figure 9: Surface of a test piece after frame averaging in order to mitigate environmental effects.

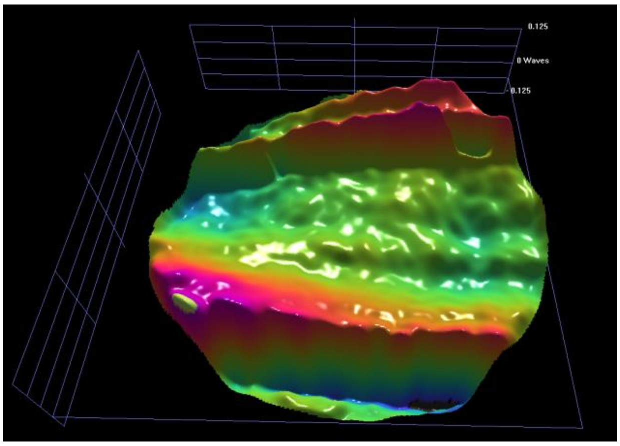

Figure 10: Single frame surface of a test piece experiencing large vibrational effects.

Although Figures 9 & 10 are of the same optical part, the surface experiencing vibrational effects (Figure 10) is incomparable to the actual surface (Figure 9). In Figure 10, the wave like pattern traveling along the surface is in fact the vibrational waves themselves and completely alter the appearance of the optic, providing inaccurate readings. Vibrations, although detrimental to the readings can be easily mitigated. The implementation of an actively supported optical table is widely used as it significantly reduces the effect of vibrations, allowing for a more stable set of readings. Another effective procedure is to take multiple sets of readings and average the results, this will remove a large portion of the effect from vibrations. But if a truly accurate set of data is required, both of these methods should be combined in order to mitigate the effects of vibrational waves.

Another main environmental effect is that caused by thermal air currents. This can be caused by change in temperature in the room or from the heat being emitted by a person standing near the part under test. The effects from thermal air currents are shown in Figure 11.

The surface shown in Figure 11 is of the same test piece used in Figure 9. The underlining pattern of the surface is clearly present, but due to the effects of the air currents, Figure 11 has been deformed into something that fails to accurately represent the surface. Much like the vibrational effects, this environmental effect can be largely reduced through the averaging of multiple data sets. Other methods to reduce thermal air current is to protect the testing area with a cover to mitigate environmental effects or to circulate the air in a predictable manor so that it can be accounted for. The efficiency of using a cover has been tested in this report and its results are given in section 5.3.

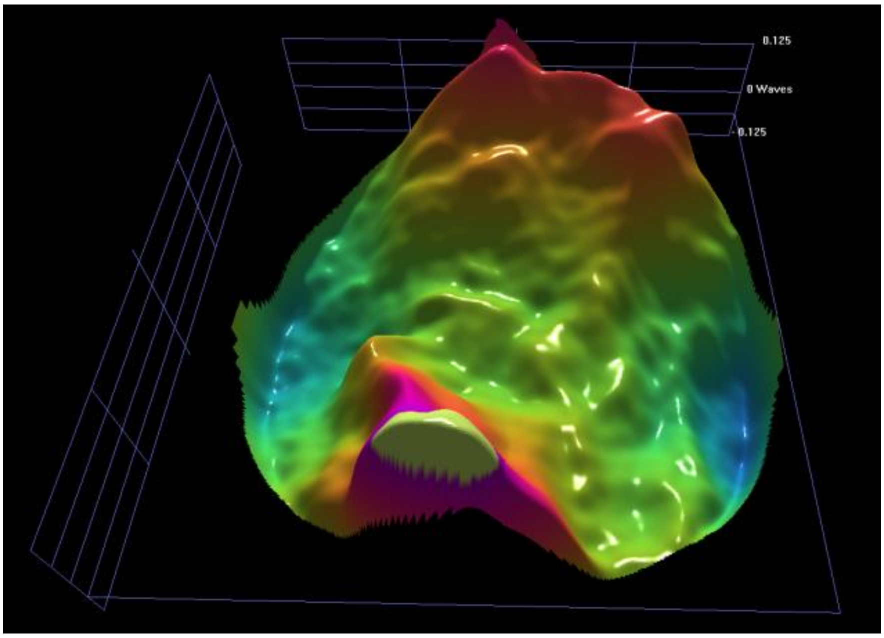

Figure 11: Single frame surface of a test piece experiencing the effects of thermal air currents.

2. Bath Interferometer Design & Construction

2.1 Bath Interferometer Design

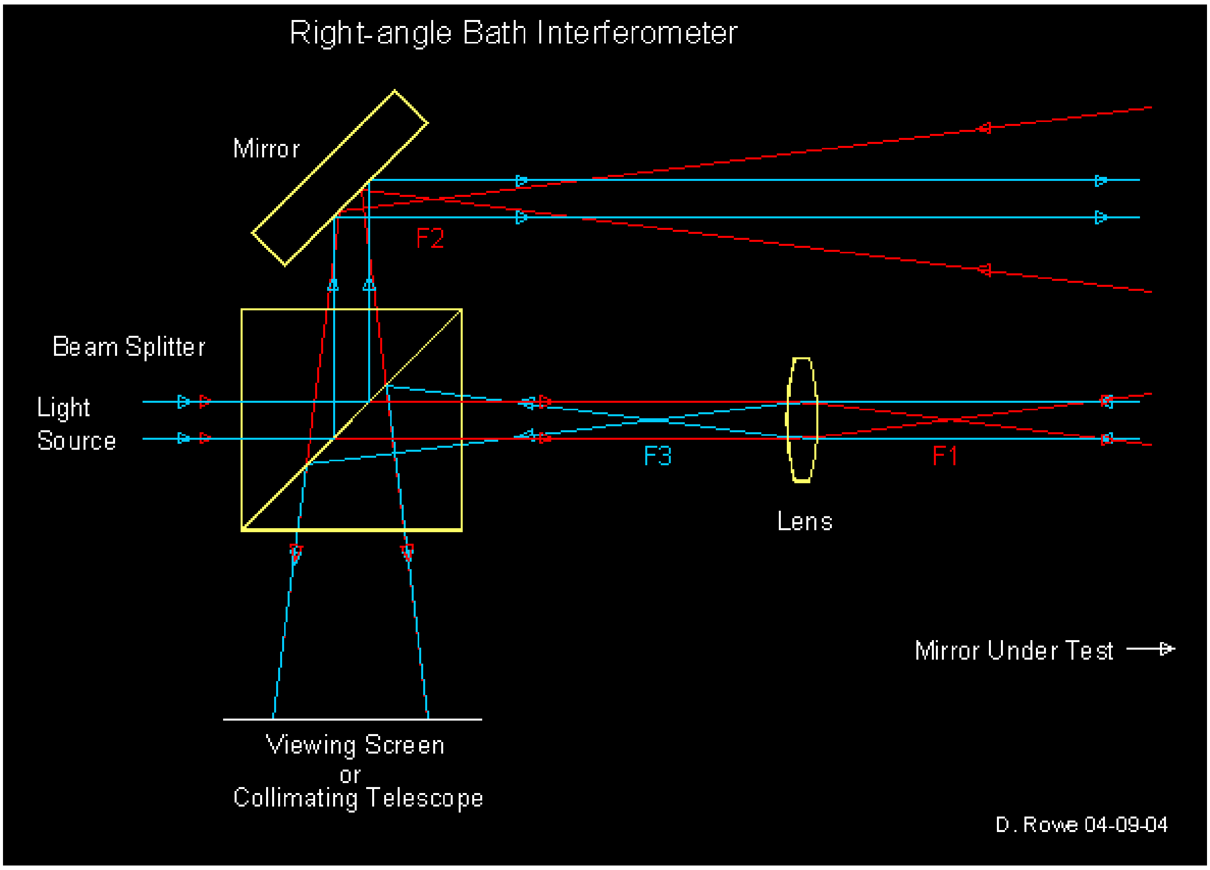

Figure 12: Bath interferometer configuration.
Credit MediaWiki

The Bath interferometer is of a very simplistic design, requiring very few components to construct a working interferometer. It is compact, highly adjustable and has a versatile design allowing to keep construction cost to a minimal without sacrificing accuracy.

Figure 12 depicts a right-angle version of the Bath interferometer. A collimated light source is divided by the beam splitter into the (blue) reference beam and the (red) test beam. The reference beam hits the mirror under test, reflects from this surface, passes through the lens and comes to a focus at F3. As for the test beam, it is expanded into a spherical wave by the lens, which has a focus at F1. The expanding beam illuminates the mirror being tested and comes back to focus at F2. The two expanding beams pass back through the beam splitter and interfere at the detector.

The Bath interferometers design allows the interferometer to be extremely compact and also allows components to be exchanged with simplicity. This is vital, as measuring different size optics requires diverging lenses of different focal lengths. The design of the Bath interferometer allows for the diverging lenses to be exchanged effortlessly, resulting in it being very practical in this sense. Due to its layout as represented in Figure 12, the interference pattern can be captured in a multiple of ways. For example a viewing screen could be placed where the two beams interfere and then an image captured manually. More practically though, a webcam can be directly placed where the test and reference beams interfere and if aligned correctly, a live feed of the interference pattern can be viewed through a laptop. Using a webcam has multiple benefits, such as significantly reducing the time to obtain a set of data as once the image is captured, it can be analysed within seconds.

With the targets set, a prototype Bath interferometer was constructed with the goal of keeping cost down without sacrificing significant accuracy. An image of the prototype is shown in Figure 13.

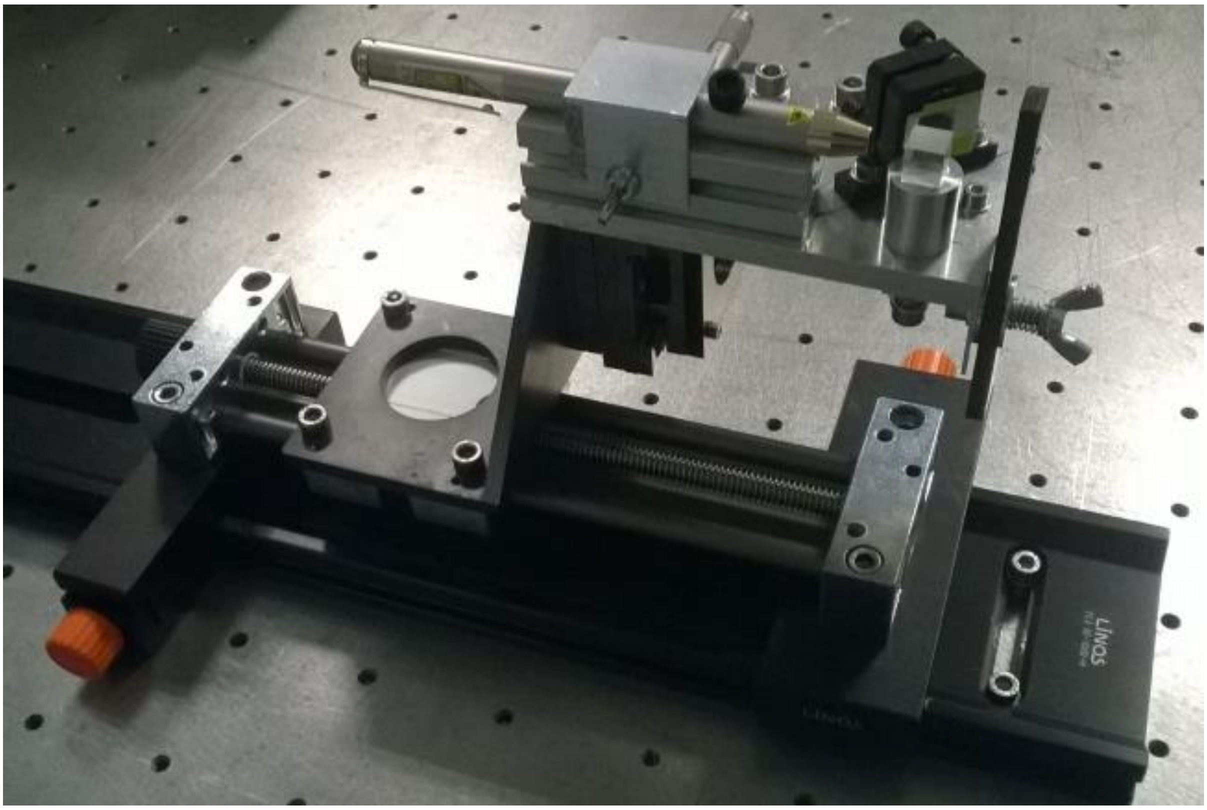

Figure 13: Bath interferometer prototype.

The prototype was constructed with the goal of making components easily accessible and replaceable, allowing components to be exchanged if underperforming. This resulted in sacrificing device compactness for accessibility. As visible in Figure 14 all the key components are visible. Each component selected will be discussed in section 2.2 along with the reasoning for each choice.

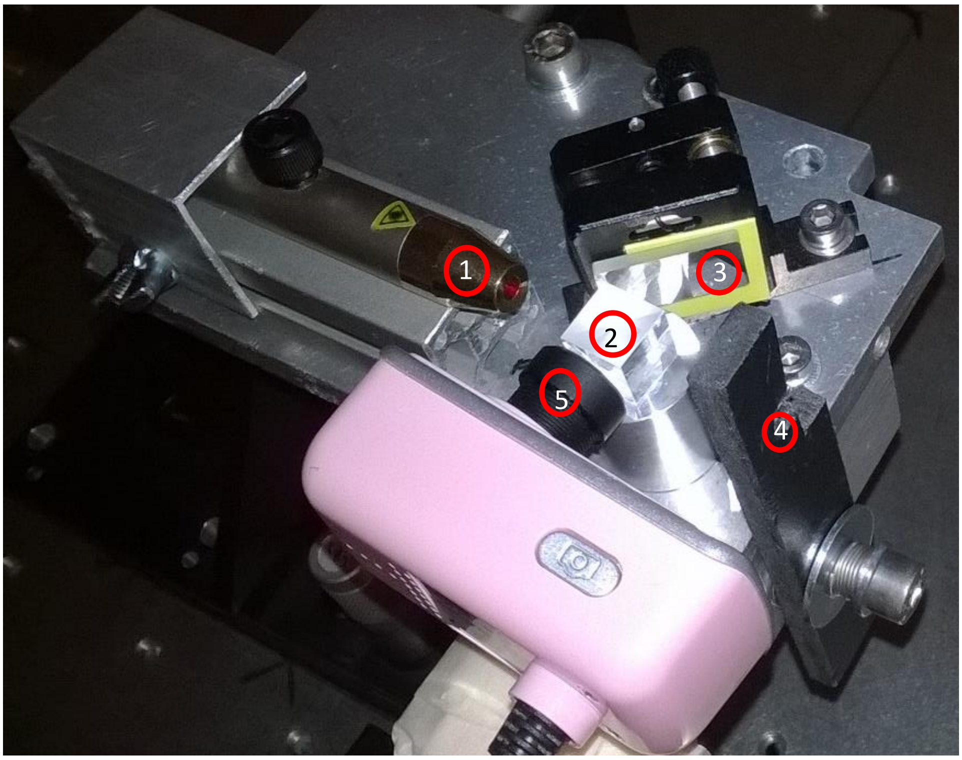

Figure 14: Image of key components in the Bath interferometer prototype

Figure 14 is an image of the key area in the Bath interferometer. It shows the light source (1) the beamsplitter (2), reference mirror (3), diverging lens (4) and the camera (5). This small region is where all the light manipulation occurs. One of the major benefits of the Bath interferometer is because to its simplistic design and accessibility, components can be easily replaced. This region is extremely compact, with all the ray manipulation occurring within and area of $4cm^2$. This is of a great benefit for two major reasons, the first being that it allows for a more compact device but secondly and more importantly, the smaller the separation between the reference mirror and beamsplitter, the less astigmatism the will be added to the system from the Bath interferometer **[1]**.

2.2 Construction

Working alongside Dave Thompson, I assisted in the construction the Bath interferometer prototype to be used in this experiment. The Bath interferometer prototype was assembled using the guidelines provided by the work of Michael S. Scherman **[1]**.

The Bath interferometer is common path, meaning that only a small part of each component is used. This leads to the assumption that because only a small section of each optical component is used, their contribution to the whole system error is very small. This means that only a small segment of each component has to be up to the required specification, leading to cheaper component cost. The Bath interferometer comprises of 5 key components and 5 alignment components. The key components being the light source, beamsplitter, diverging lens, reference mirror and webcam. With only using these 5 key components, an operational Bath interferometer can be constructed. But for a usable and practical device, alignments components are just as vital as the key components. Each component is further broken down and discussed in this section.

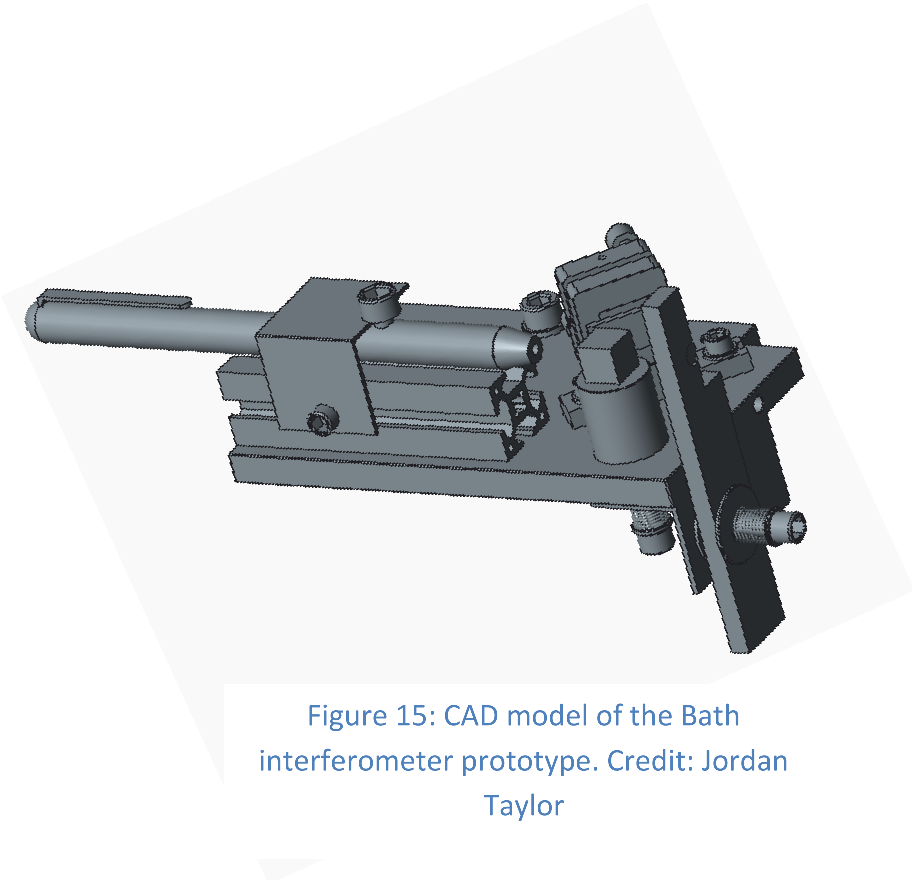

Figure 15: CAD model of the Bath interferometer prototype. Credit: Jordan Taylor

2.2.1 Alignment Components

When dealing with light interference, getting all the components aligned correctly in order to observe the resultant interference pattern is the most challenging part of the measurement process. The result of misalignment is the absence of an interference pattern meaning readings cannot be obtained. Alignment components such as Micrometers allow for interferograms to be more easily obtained and results in a more efficient alignment process.

There are 5 components that allow for alignment. The largest is a rail that the Bath interferometer rests on and allows for large lateral movement. This is key as the Bath can simply be moved to the vicinity of the focal point of the mirror under test. Once in this region, more precise alignment is required. This is where components with more precise lateral and longitudinal adjustments are required. Two Micrometers Positioning Stages have been utilised in order to achieve this, one allowing for longitudinal traverse, and the other vertical traverse. Between these components the Bath interferometer can be aligned to the correct location. The other two components are for internal alignment. The first component is one of a rotary nature and allows for the rotation of the beam splitter. The second allows for fine adjustments in the reference mirror. These two components are required for the initial internal alignment. But once internally aligned, the Bath will not need to be internally realigned for separate test optics as this alignment is done externally.

2.2.2 Light Source

For a high precision metrology instrument, it might be expected that a high class stabilised laser would be required to achieve the required accuracy. But this has been reported not to be the case for the Bath interferometer **[1]**. The light source used in the Bath interferometer prototype is just a simple 652nm laser pen that can be simply and cheaply acquired from numerous places. As long as the wavelength of the light stays stable throughout the measuring process, high accuracy reading can be procured. The laser pen was tested for its wavelength stability with a spectrometer (Ocean Optics USB 2000+ Spectrometer) and a sample of the results are shown in Graphs 1 & 2.

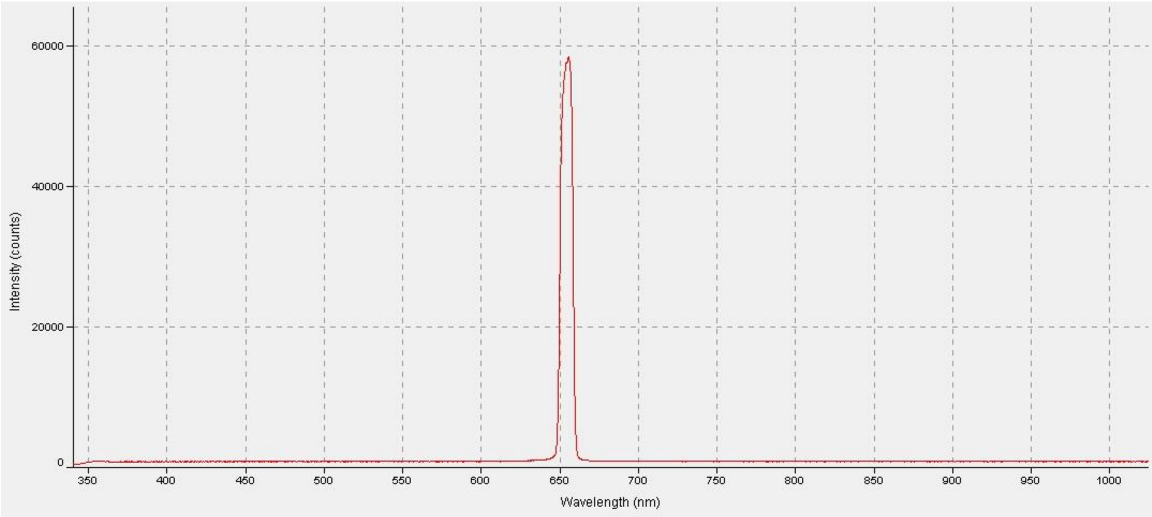

Graph 1: A spectrograph of the laser pen wavelength intensity. This graph represents a reading taken at t = 0min.

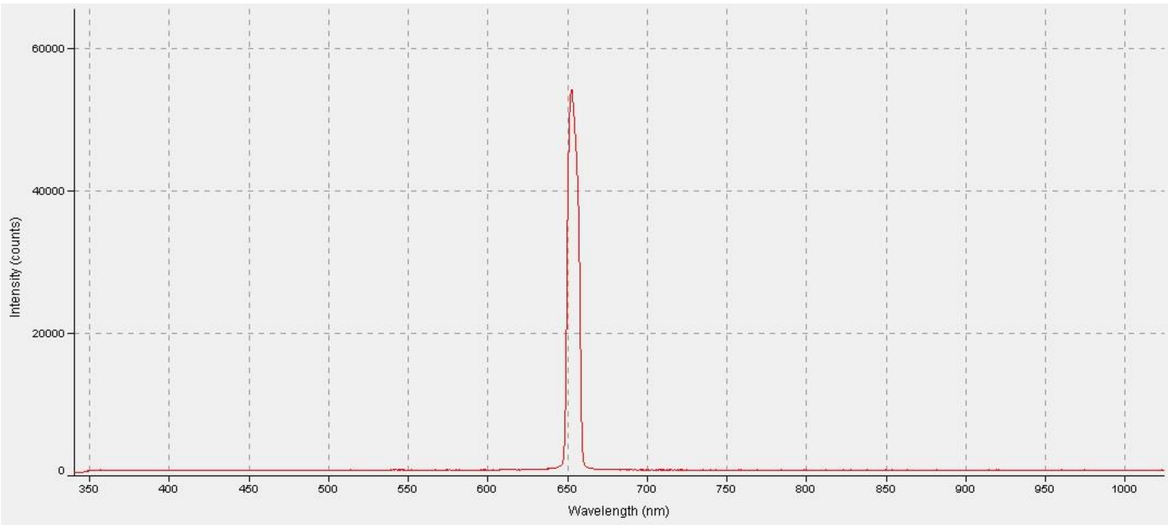

Graph 2: A spectrograph of the laser pen wavelength intensity. This Graph represents a reading taken at t = 30min.

The readings were obtained over a short period (seconds) at intervals of 10 minutes over a time frame of 40 minutes, which is representative of the period it takes to obtain a data set. Readings obtained at t = 0 and t = 30 minutes are shown in Graphs 1 & 2. As revealed, over the period this test was conducted the laser's wavelength did not vary significantly from 652nm. The change in intensity arises from the laser being at different distances from the spectrometer whilst the readings were being obtained and is not a representation of laser intensity fluctuations.

The light source proved to be more than adequate during the main experiment, but in order to confirm the light source did not impair the results, tests with a calibrated light source is required, but unfortunately such a light source was not procurable.

2.2.3 50:50 Cube Beamsplitter

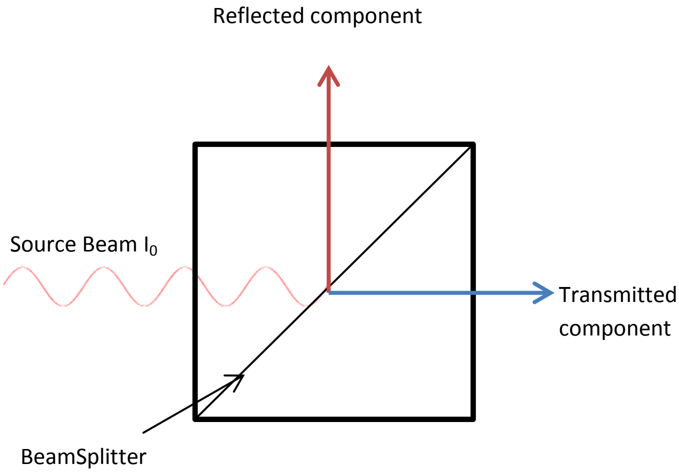

Figure 16: Diagram of a beamsplitter

A beamsplitter cube (Figure 16) consists of two right angle prisms, where the widest face has a beam splitter coating applied, in this case a 50:50 splitter coating. The beamsplitter is the component that splits the source light beam (I_0) into two beams with equal intensities, one being transmitted and the other reflected.

$$I_0 = I_1 + I_2 = \frac{1}{2}I_0 + \frac{1}{2}I_0 \qquad (1)$$

A beamsplitter that accurately splits the light source into two even beam is vital. If the source beam is not evenly split, the result will be an interference pattern that represents a false surface. Although the 50:50 cube beamsplitter can be coated or uncoated, a coated part was chosen as it helps to reduce ghost fringes **[1]**.

2.2.4 Biconvex Lens

A biconvex lens is used to expand the test beam so that it covers the test optic aperture. This component will need to be changed for optics with different focal lengths and sizes. The ability to interchange diverging lenses is needed because if the test beam is expanded larger than the test optic's full aperture, the intensity of the light reflected back will be too low to acquire results from. This means that good accessibility to the diverging lens is required.

The lens must give out a spherical wavefront in order to obtain accurate results. It is assumed that this is true for the selected lens but no tests have been conducted to verify this. The biconvex lenses will also need to have no irregularities, otherwise errors will be added to the reading. The biconvex lens used in this prototype was acquired from a low cost webcam and has proved to be more than sufficient. It expands the beam efficiently and evenly allowing for the test optics used in the main experiment to be fully enclosed in light.

2.2.5 Reference Mirror

The reference mirror is one of the components that cannot be undervalued. Although it is impossible to obtain a mirror with an absolutely flat surface, a reference mirror with an extremely low surface form error is vital to prevent adding errors into the measurement of a test optic. When the reference beam is reflected off the reference mirror, it will carry any surface irregularities it encounters and these errors will be induced in the final interferogram of the test optic.

The mirror used in the Bath prototype has a dimension of 2cmx4cm with a surface RMS of around 80nm (Figure 17). This is extremely high, but it is important to remember that the light will only be interacting with a small portion of the reference mirror. To test the reference mirror's surface form, a virtual circular mask with a diameter of 4mm was created within 4Sight and moved around the surface in order to obtain an idea the RMS values over a small region. The mask is shown in Figure 18. The RMS values within the mask varied between 2nm to 6nm when moved to different locations. From previous research, this surface flatness will be sufficient **[1]**. It is also important to note that realistically, the light will not be interacting with a region more that 2mm in diameter.

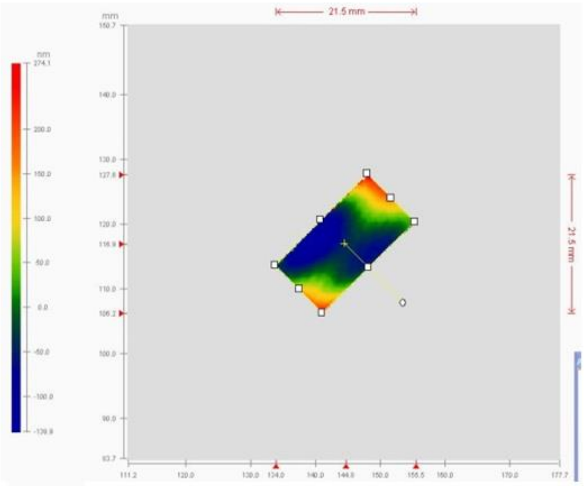

Figure 17: Interferogram of the reference mirror as seen in 4Sight. Taken with the 4D Phasecam 6000 interferometer

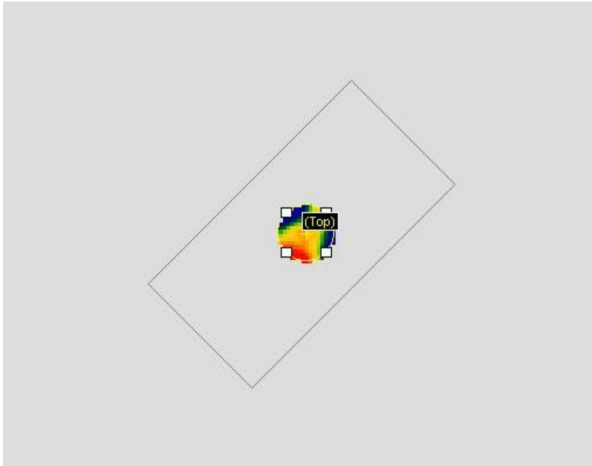

Figure 18: Surface map of the reference mirror with a mask highlighting the laser interaction area. 4D interferometer used to take readings and 4Sight used as an analysis tool.

2.2.6 Camera

In the Bath interferometer prototype, a webcam attached to a laptop is used to capture an image of the interferogram. Although the interferogram can be captured in multiple ways, having the two beams travel directly into the webcam has proven to be extremely effective. This allows for the user to view the interferogram directly on the monitor allowing for a faster image capturing process. An image of 800x600 pixel resolution is required for the analysis, meaning that almost all current webcams are more than capable of being used for this application. This results in the imaging component of the interferometer being very low cost. There have also been discussions about adding a docking station for a smart phone to be placed allowing for images to be captured more freely. This option is currently being further explored and no conclusion has been drawn from this idea yet.

2.2.7 Prototype Construction Cost

The Bath interferometer prototype used in this report had a construction cost of £121.40. This cost excludes alignment components but includes all the components required for a working interferometer. It is important to note that although this cost can be considered low, it was built with readily available components meaning one could build a Bath interferometer for much less. It has been estimated that a Bath interferometer of the same design can be constructed for a little as £30 if components are purchased from more competitive suppliers. This shows that the Bath interferometer can enter the market as a low cost interferometer as initially predicted.

Table 1

Part	Quantity	Unit cost (£)	Supplier
Beamsplitter	1	66.61	Qioptiq
Mirror	1	5.80	Stanwax Laser
Mirror mount + Mounting kit	1	29.00	Stanwax Laser
Biconvex lens	1	4.00	N/A
Webcam	1	7.00	Ebay
Laser	1	7.99	Maplins
Total Cost		121.40	

2.3 Technological Limitations

The Bath interferometers design leads to instrumental astigmatism being added to the readings. This inherent astigmatism is well-documented and can be calculated by the following equation

$$OPD = \frac{D^2 d^2}{16R^3} \qquad (2)$$

D is the diameter of the mirror under test, d is the beam to beam separation, R is the radius of curvature of the mirror and OPD is the optical path difference the longest and shortest paths to the mirror.

The inherent astigmatism along with other system induced errors can be removed by rotating the mirror and obtaining readings at different orientations. This procedure has been implemented in this report and is further discussed in Section 4. When obtaining results, it was revealed that the wavefront of the reference beam becomes inverted depending whether the interferometer is inside or outside the focal point of the test mirror. Although this is not of surprise, it can become problematic if ignored. To obtain the correct surface readings, the interferometer needs to be placed outside the focal length in order to obtain the correct wavefront.

2.4 Software Packages

One of the major appeals of the Bath interferometer is that the software packages required for interferogram analysis are freely downloadable. There are multiple software packages to select from but the two stand out packages are OpenFringe and FringeXP **[7]**. The software package selected and utilised for this experiment was OpenFringe. Although this software has a fraction of the capabilities of that available in 4Sight, OpenFringe has an extremely user-friendly interface and allows for efficient and accurate interferogram analysis.

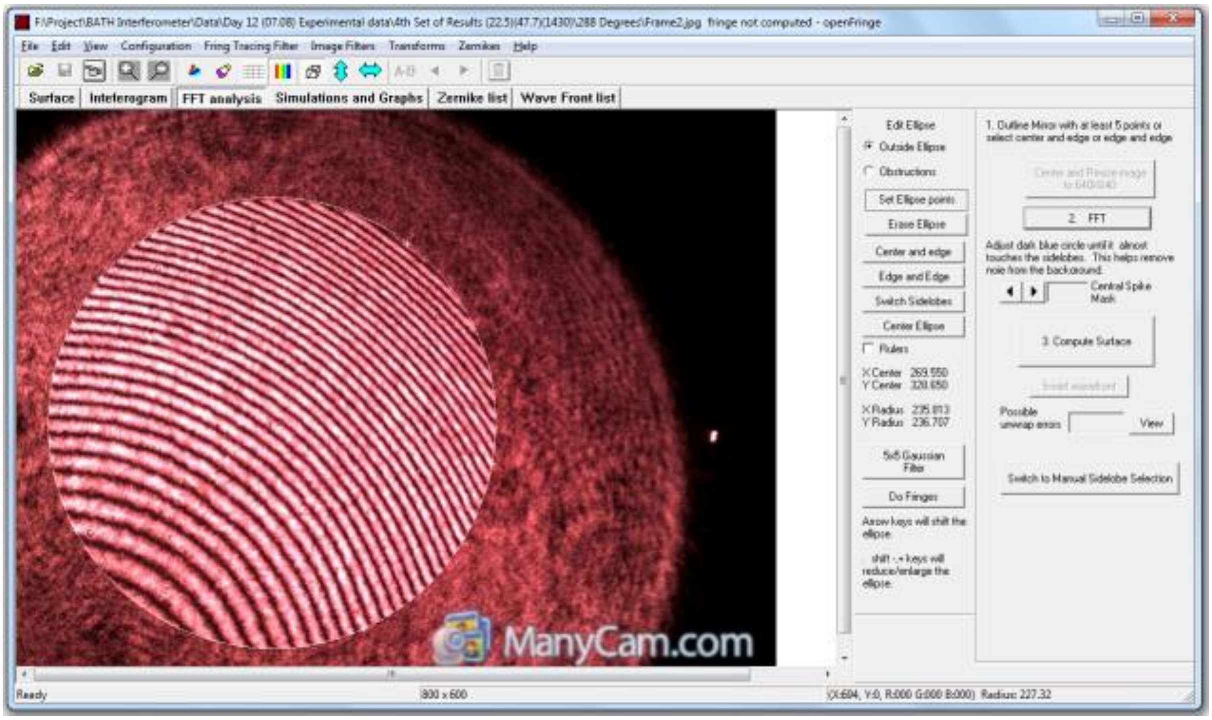

Figure 19: Interference fringe pattern produced by a Bath interferometer. OpenFringe is the analysis tool being used.

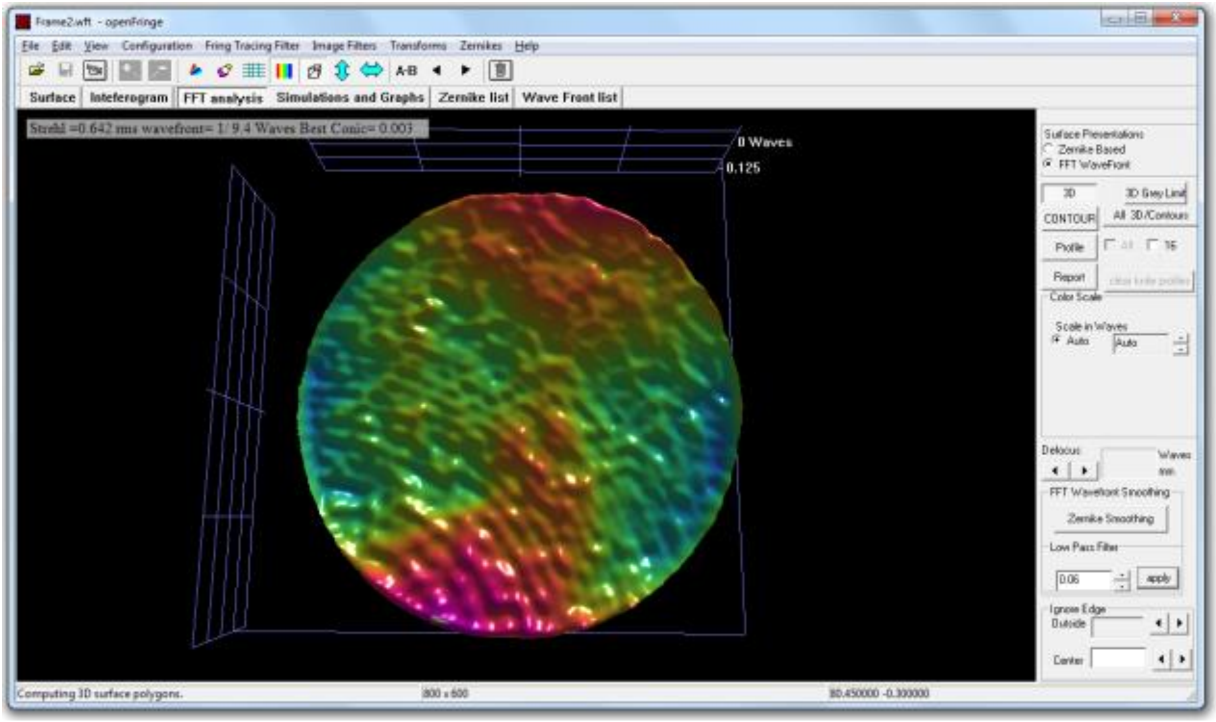

Figure 20: 3D interferometric map of spherical mirror. A Bath interferometer was used to take the reading and OpenFringe used as an analysis tool.

Once an image of the interferogram is captured, it can be loaded into the software for analysis. After the interference pattern is manually identified in OpenFringe (Figure 19), FFT can be performed on the image producing a surface representation of the optic (Figure 20). This process is discussed in more detail in Section 4.1.1. OpenFringe also allows for multiple images to be analysed in batches, minimising the time required to analyse data and eliminating the need for constant human presence during analysis. Once the interferogram has been analysed, the surface map can be viewed in a multiple of ways, such as 2D and 3D, shown in Figures 21 & 20 respectively.

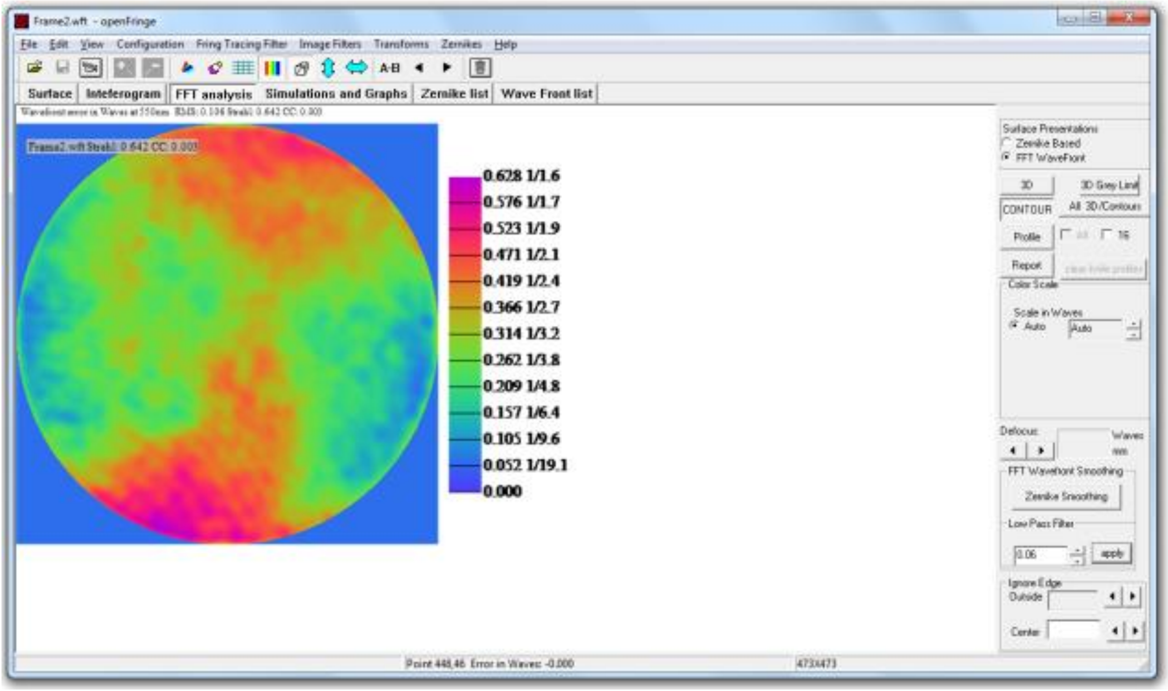

Figure 21: 2D map of spherical mirror. A Bath interferometer was used to take the reading and OpenFringe used as an analysis tool.

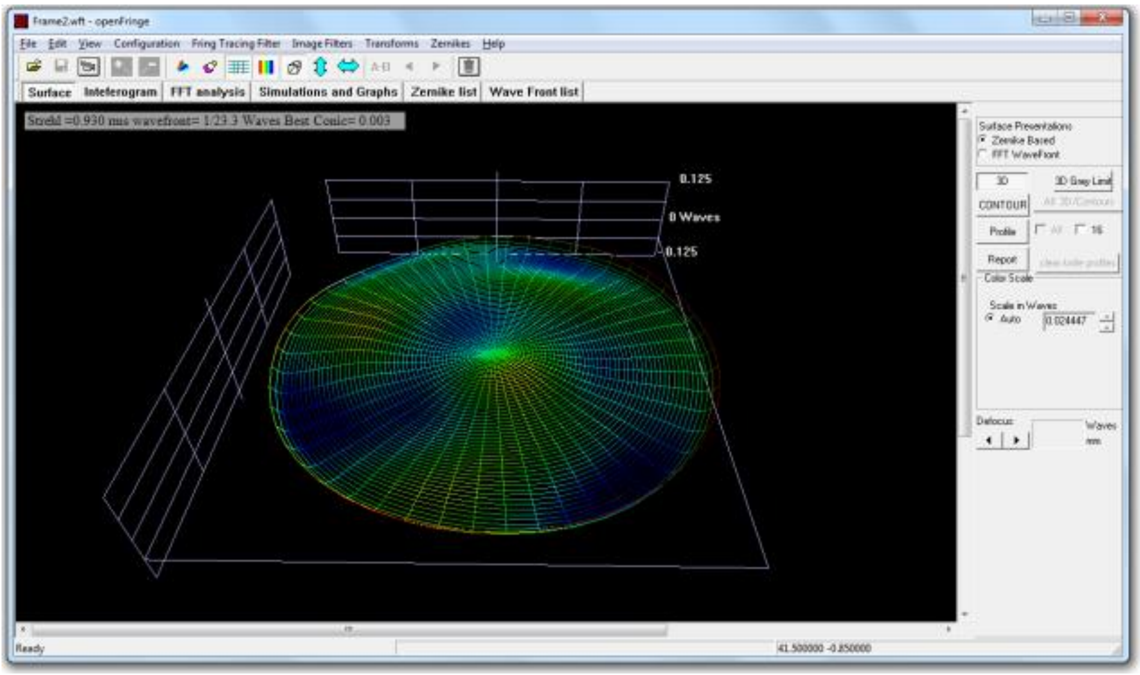

Figure 22: Zernike map of spherical mirror. A Bath interferometer was used to take the reading and OpenFringe used as an analysis tool.

One of the more important features of OpenFringe is the ability to view the Zernike coefficients for the optical surface. This allows for the comparison of the Zernike coefficients between the Bath and 4D interferometers. OpenFringe provides the coefficients for the first 42 Zernike terms in units of wavefront (550nm wavelength waves). OpenFringe also provides the ability to map the surface using the Zernike values as demonstrated in Figure 22.

As previously discussed, the Bath interferometer design inherently adds astigmatism to the results. The value of the inherent astigmatism added can be calculated (refer to Section 2.3). OpenFringe has a function that calculates astigmatism and may remove it from the results, thus eliminate this error from the measurements. Although this feature has not been used in this report, it is useful when analysing wavefronts as it negates one of the major drawbacks with Bath interferometer technology. OpenFringe also has a function that can calculate the amount of astigmatism induced by the test stand. Along with the points discussed, OpenFringe also has multiple features that could prove to be useful in other scenarios such as the ability to calculate, through sufficient experimentation, the errors inputted by the test stand and has the ability to plot graphs of the surface deviation along the x and y planes.

2.5 FRED Model of the Bath Interferometer

FRED is an Optical Engineering Software capable of simulating the propagation of light through any optomechanical system by raytracing. In order to compliment the prototype, an optical model of the Bath interferometer has been created using FRED.

This model provides a more detailed understanding of the Bath interferometer optical layout and in turn provides better insight into how the Bath interferometer works. Figures 23 & 24 demonstrate how the rays propagate through the model. The model also provides the ability to identify what diverging lens is required for optics of different shapes and sizes by just changing the dimensions of the test piece within FRED. This would minimise the time it would take to identify the correct diverging lens as well as identifying the region where the Bath interferometer needs to be in order to obtain an interferogram which would in turn reduce the alignment time.

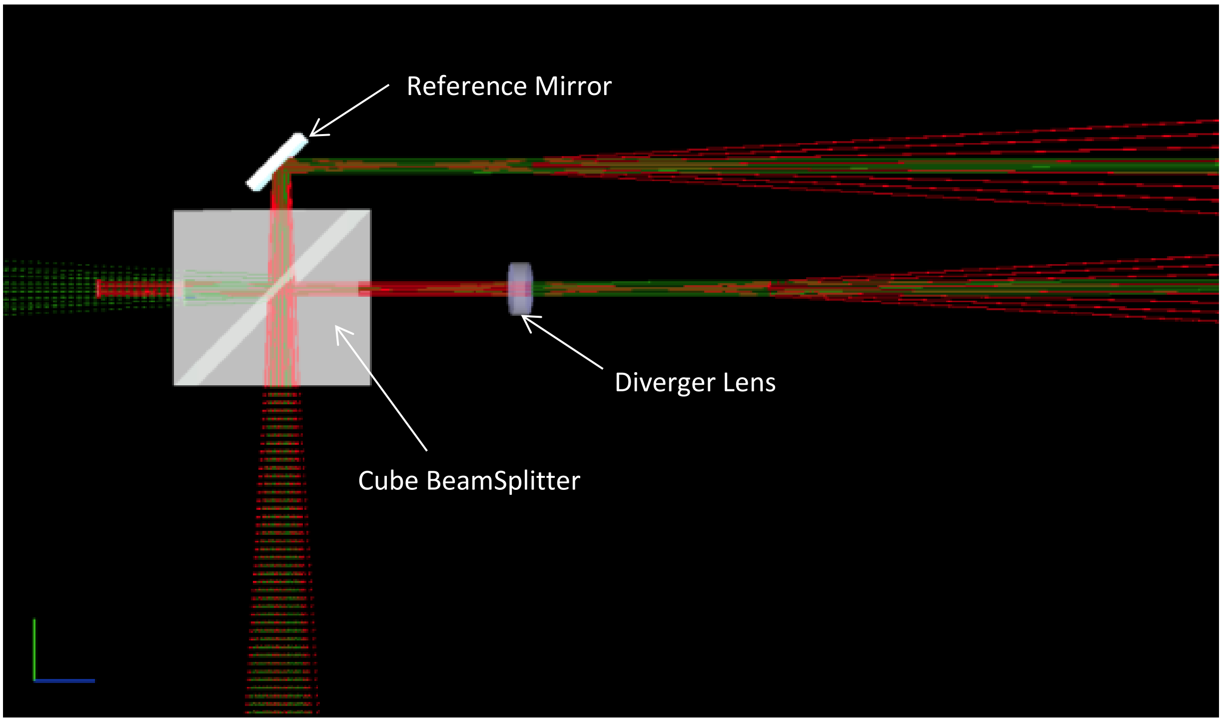

Figure 23: Optical Mechanical representation of the Test (Red) and Reference (Green) beams. This model was created using Optical Engineering Software, FRED.

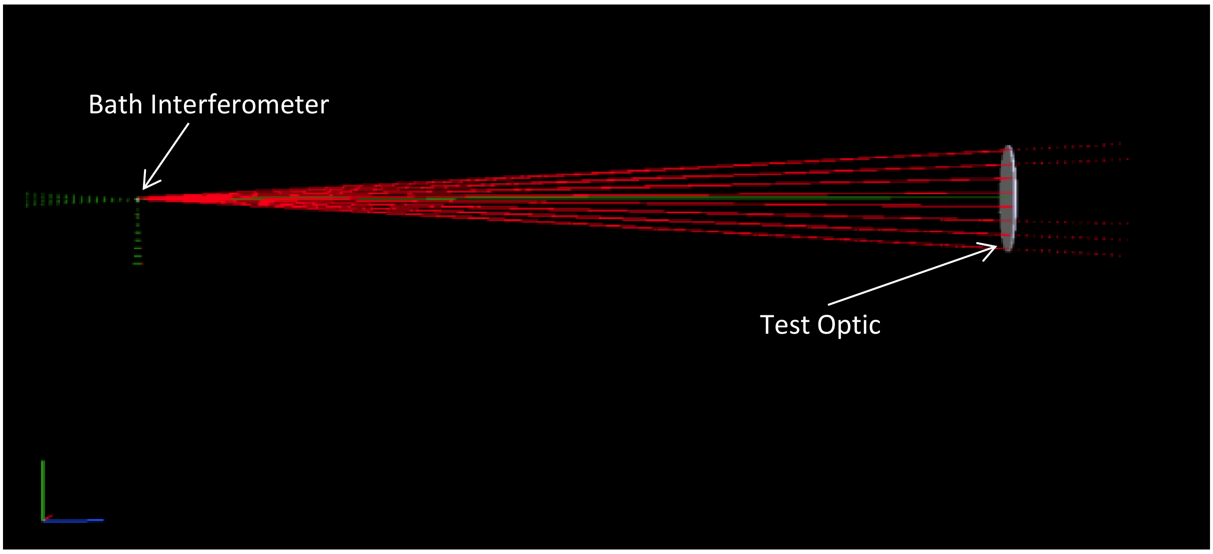

Figure 24: Optical Mechanical representation of the Bath interferometer system. This model was created using Optical Engineering Software, FRED.

3. 4D 6000 Instantaneously Phase Shifted Interferometer

The 4D Technology "dynamic" PhaseCam 6000 laser interferometer is one of the industry's leading interferometer in terms of precision, utility and efficiency. It is also accompanied by an intricate software package, 4Sight allowing for functions that very few other interferometers can achieve **[8]**. The design of the 4D interferometer is far more complex than Bath interferometer, implementing phase shifting techniques to obtain readings. Phase-Shifting interferometry is superior to raytracing and FFT analysis techniques as it is more immune to background noise. Simultaneous Phase-Shifting interferometry also allows for instant data analysis meaning you can view the surface without needing to process interferograms.

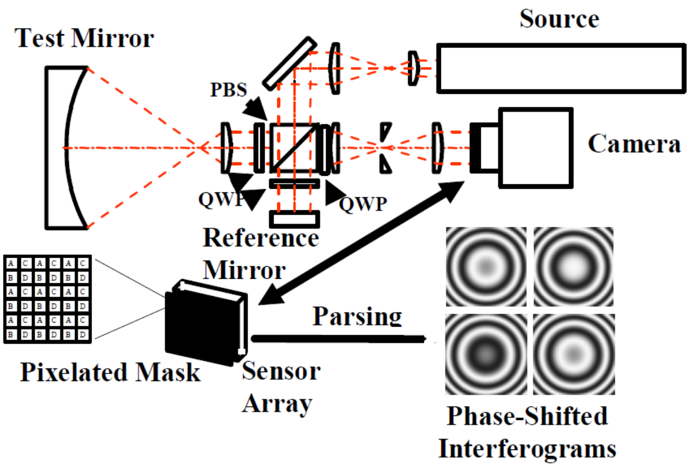

Figure 25: Twyman-Green simultaneous phase-shifting interferometer configuration **[2]**.

The 4D 6000 interferometer design is represented by Figure 25. This technique implements far more complex components than the Bath interferometer such as quarter wave plates (QWP), a polarization beamsplitter and a CCD array **[2]**. The 4D interferometers design allows for the four phase-shifted interferograms to be detected simultaneously on a single detector array **[2]**. In phase shifting interferometry, if the phase shifts are not exactly 90 degreed, it leads to errors having twice the frequency. This effect can be reduced by taking several frames of data with the average phase difference between the two interfering beams different for each frame. Interestingly, this frame averaging technique will lead to more accurate results being obtained then if there was no vibration to begin with **[9]**. These Double frequency errors can be almost fully removed in a simultaneous phase shifting interferometer. This is one of the large advantages of simultaneous phase-shifting interferometers.

4. Experimental Procedure

4.1 Obtaining Readings of Spherical Optical Mirrors

The principle of the experiment is obtain readings with the two interferometers and compare the results. The capabilities of the 4D interferometer is well documented so a comparison will lead to an understanding of the Bath interferometers accuracy. The following Section will discuss the procedure for obtaining interferometric results from two spherical mirrors, along with the procedure for the environmental experiment.

4.1.1 Bath Interferometer Procedure

To determine the accuracy of the Bath interferometer, readings from two separate optical mirrors were obtained. The dimensions and key information of the two optics are listed in Table 2.

Table 2

Test Mirror	1	2
Profile	Sphere	Sphere
Diameter (mm)	203	200
Radius of Curvature (mm)	1480	1210
F Number	F3.7	F3
Coated (yes/no)	No	Yes

Results from two different dimensional test pieces will result in a more conclusive experiment. The experimental procedures for both test mirrors were near identical in an attempt to acquire comparable results. The test apparatus was set up as shown in Figure 14. The most important part of the experimental procedure is the requirement to correctly align the Bath interferometer with the optical part under test. The Bath interferometer needs to be positioned so once the test beam is reflected, it focuses just in front of the reference mirror (F2), which is shown in Figure 12. The reference beam was then aligned so that it reflected off the centre of the test mirror into the diverging lens of the Bath interferometer. If both of these steps were properly executed, both light beams would now be roughly aligned. Once all these components were in position, only minor adjustments were required in order to view an interference pattern through the webcam. The interference pattern produced is represented by Figure 26.

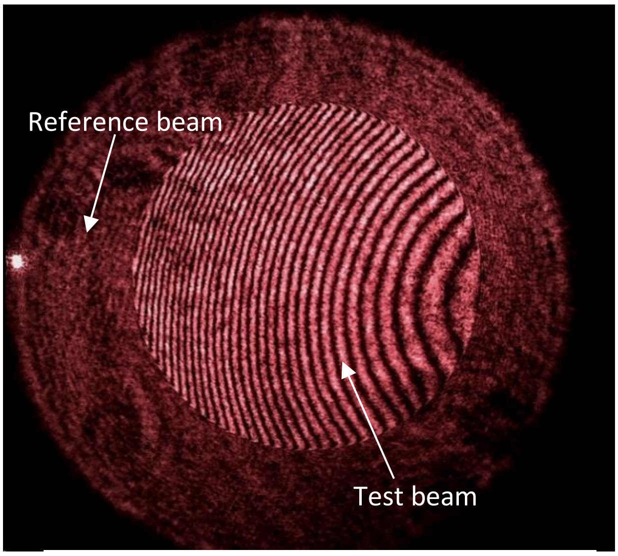

Figure 26: Interference pattern produced by a Bath interferometer.

With minor adjustments in the lateral and longitudinal directions a fringe pattern similar to that shown in Figure 26 will be obtained and ready for analysis. Is it important to note that for an accurate set of readings, the number of visible fringes desired is between 30-40 for accurate FFT analysis to occur **[1]**. The reading sensitivity is related to the number of fringes. A small number of fringes are more sensitive to surface error but a large number of fringes will lead to a surface with a better resolution. Taken to the extreme, one single fringe will tell you a lot about the area it covers (Bright lines) but no information can be obtained from where it is not (Black areas). Therefore a compromise is needed to be made.

Once the Bath interferometer was aligned, readings were obtained. To minimise the errors introduced by the Bath interferometer and test stand, the optical part was rotated 5 times in increments of 72°, with results being obtained at each rotation. Using previous work, it was estimated that 20 readings at each rotation would be sufficient for accurate readings **[1]**. Meaning that for 1 set of results, 100 images were obtained (20 for each rotation: 0°, 72°, 144°, 216°, 288°). Once a set of readings were taken, the results were analysed. As mentioned, OpenFringe was utilised to process the interferograms produced from the Bath interferometer. Each image underwent FFT analysis (Figure 27) followed by a surface computation which resulted in a contour map of the surface being produced.

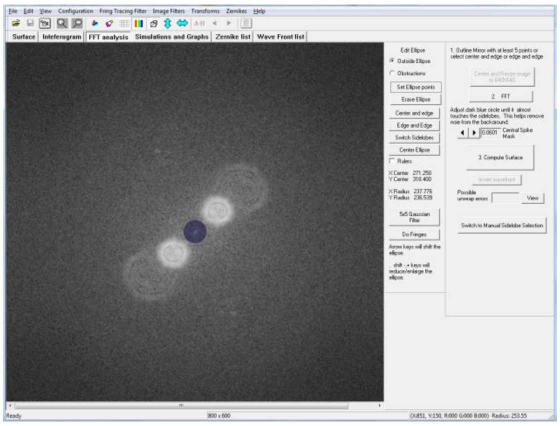

Figure 27: FFT analysed data from a spherical mirror. A Bath interferometer was used to take readings and OpenFringe used as an analysis tool.

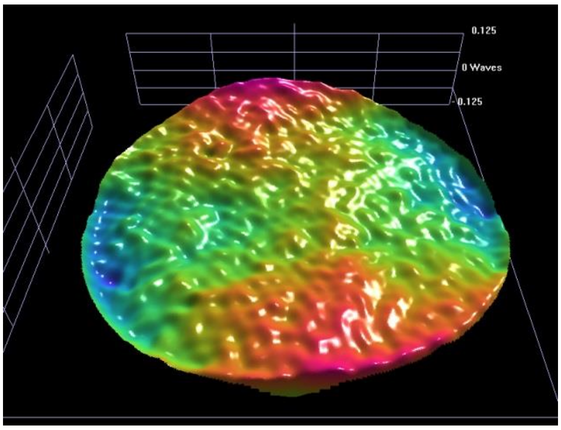

Figure 28: 3D map of spherical mirror once the FFT data is computed. OpenFringe used as the analysis tool

Once all 20 images at each rotation had been analysed, OpenFringe was then used to average the readings from each rotation. As discussed in Section 1.5 this process significantly reduces the environmental error caused by vibrations and thermal air currents. One all the readings at each rotation had been averaged, OpenFringe was used to artificially de-rotate the surfaces. This artificial de-rotation is necessary is order to get all the surface readings to the same orientation so a final average can be obtained. This single final map will represent the surface of the part that should exclude the significantly errors introduced by the test stand, the Bath interferometer and environmental effects. 10 sets of results were obtained for the 203mm diameter test mirror and 5 sets for the 200mm diameter test mirror. The results acquired are represented in Section 5. An in-depth calibration can be found in Michael S. Scherman's work **[1]**.

4.1.2 4D 6000 Instantaneously Phase Shifted Interferometer Procedure

The procedure of acquiring data with the 4D interferometer was intentionally made similar to that of the Bath interferometer. The 4D interferometer was used to obtain readings of the same two test pieces (Table 2). The test apparatus was set up as shown in Figure 30. The 4D interferometer has a very different alignment process to the Bath interferometer. Due to its Phase shifting technique, it is vital to null out the fringes on the interferogram otherwise they will add unwanted errors to the reading (Figure 29). Once the 4D interferometer was aligned and the fringes had been nulled, readings were procured. Although the 4D interferometer can obtain readings at a much faster rate, the same amount of readings were taken in order to achieve a fairer test of interferometer quality. 20 frames of the surface was obtained at each orientation (0°, 72°, 144°, 216°, 288°) to be averaged and compared. Although the surface rotations are no as necessary as they are for the Bath interferometer, they still help in reducing system and environmental errors. A major advantage of the 4D interferometer is that there is no need to manually process interferograms in order to get a surface map of the optic, this process is automatic. 4Sight allows for the surface to be viewed via a live feed as all the light interference analysis is done instantaneously, thus the name 'instantaneously phase shifted interferometer'. Once all the data for each orientation had been obtained, they were artificially de-rotated and averaged within 4Sight. Once both data sets had been procured, the results were compared in an attempt to gain insight into the accuracy of the Bath interferometer.

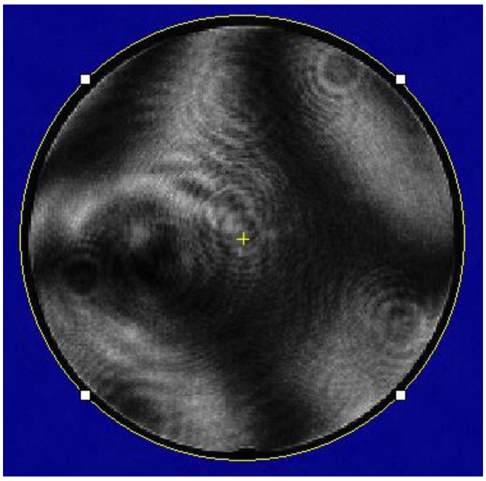

Figure 29: Interference pattern produced by a 4D interferometer.

Figure 30: Experimental setup for the 4D interferometer.

4.2 Testing Environmental Effects Procedures

4.2.1 Thermal Air Currents

A minor side experiment was conducted with the purpose of gaining insight into the Bath interferometers sensitivity to thermal air currents. For this experiment a shroud was constructed with the sole purpose of protecting the test from thermal air currents. If the shroud works as expected, the affect thermal air currents have on readings should be almost fully mitigated, resulting in more accurate readings. The Bath interferometers sensitivity will be tested by obtaining two data sets, one with the apparatus covered with the shroud, the other without. The experimental apparatus can be viewed with and without the shroud in Figures 30 & 31. A data set consists of 10 frames at the same orientation. There is no frame averaging or part rotation in this experiment as it is not a surface that is being tested, but the variation in readings. Firstly readings were obtained without the shroud. This was conducted by taking readings 5 seconds apart in order to let the environment change. Once 10 readings had been obtained, the shroud was placed over the test apparatus and results were obtained in the same manner as before, 10 frames 5 seconds apart. Once the results were obtained, the deviation in frames of the two sets of data was analysed in order to obtain an insight into the Bath interferometers sensitivity to thermal air currents.

Figure 31: Experimental setup for the 4D interferometer protected by a shroud.

4.2.2 Temperature

Due to the duration it takes to obtain a set of readings, maintaining a constant temperature throughout testing is vital. An increase in temperature causes an increase in the thermal air currents which will lead to inconsistent environmental conditions throughout testing, - potentially inducing errors into interferometric measurements due to a distorted wavefront being returned to the camera. Even though the implications of thermal air currents are reduced through data averaging, a change in the initial condition can cause small deviations in the readings that will lead to an inconsistent experiment.

In an attempt to mitigate this effect, testing was conducted at the same time each day to reduce any effects in temperature that the building environmental controls might have had. To confirm that the temperature maintained constant throughout testing, an environmental sensor (TinyTag) was deployed during testing to obtain readings of the local temperature and humidity levels.

Graphs 3 & 4 show that the temperature maintained within 1 °C throughout testing. The obtained results are within reasonable deviation, meaning that effects from temperature deviations were kept to a minimal.

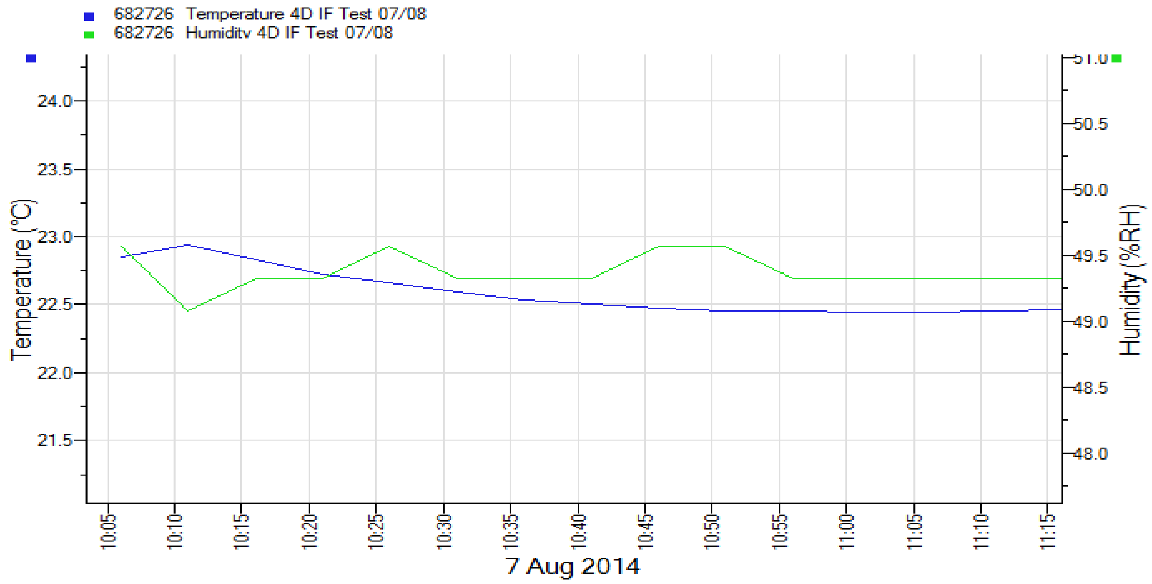

Graph 3: Data produced from environmental sensor. Readings obtained over a period of 24hrs and shows temperature and humidity variations.

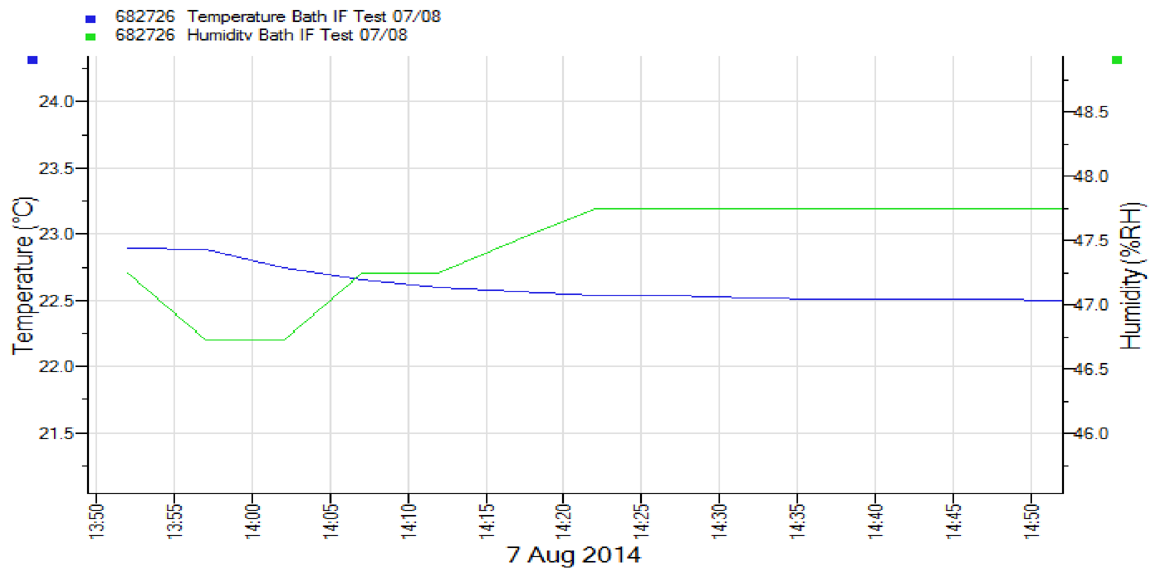

Graph 4: Data produced from environmental sensor. Readings obtained over a period of 1hr and shows temperature and humidity variations

To obtain an insight into how much the temperature deviates in the testing room over a period of 24hrs, the sensor was deployed overnight to observe the temperature variations and the results are shown in Graph 5. Over a period of 24hrs there was large fluctuations in temperature and humidity. This could be attributed to the air conditioning system being switched off at night along with other factors. These reading further support the need for swift and controlled testing.

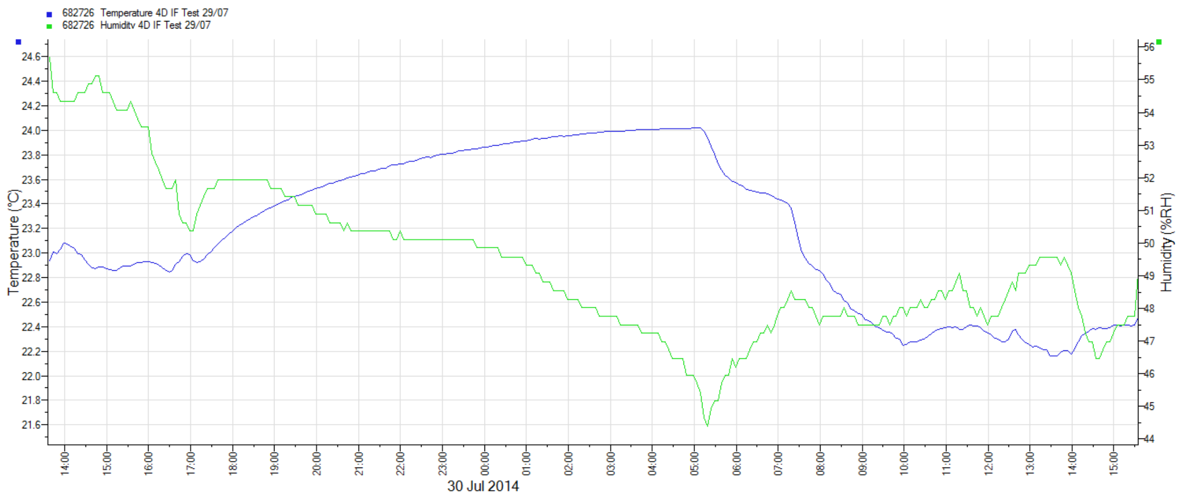

Graph 5: Data produced from environmental sensor. Readings obtained over a period of 24hrs and shows temperature and humidity variations

5. Experimental Data & Results

5.1 203mm Diameter Uncoated Spherical Mirror

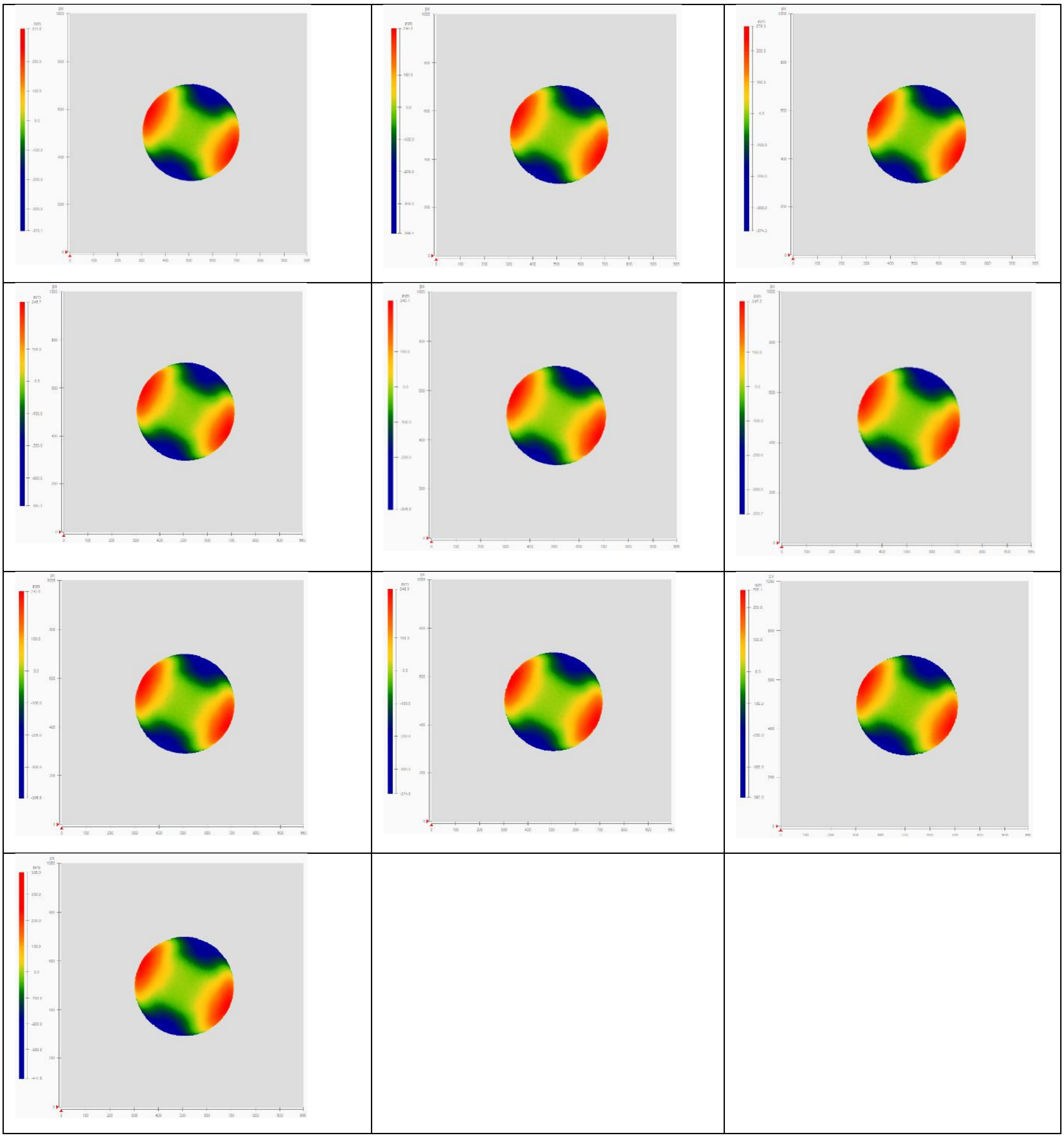

Figure 32: Surface readings obtained with the 4D interferometer of the 203mm spherical mirror. The RMS value of each set is represented by in Table 3 and the Zernike coefficient values can be found in Section 11.1.1.

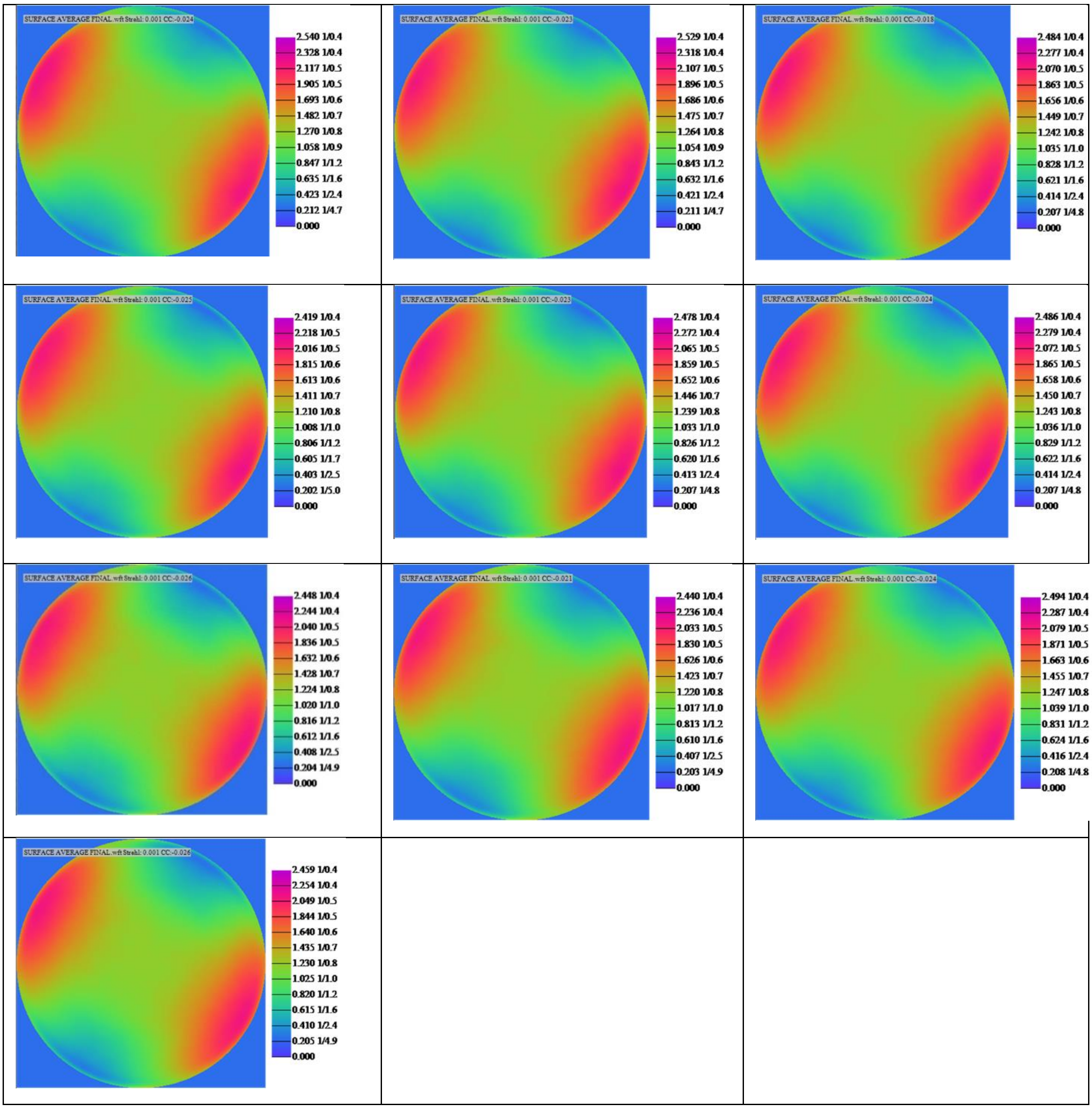

Figure 33: Surface readings obtained with the Bath interferometer of the 203mm spherical mirror. The RMS value of each set is represented by in Table 3 and the Zernike coefficient values can be found in Section 11.1.2.

Table 3 – RMS values obtained for each set with each interferometer

Set	RMS Value obtained with the Bath (nm)	RMS Value obtained with the 4D (nm)
1	119.57	119.5
2	119.57	118.8
3	114.58	118.4
4	114.58	118.8
5	114.58	116
6	114.58	118.2
7	114.58	118.7
8	114.58	118.7
9	114.58	119.9
10	114.58	118.2
Average	115.58	118.52

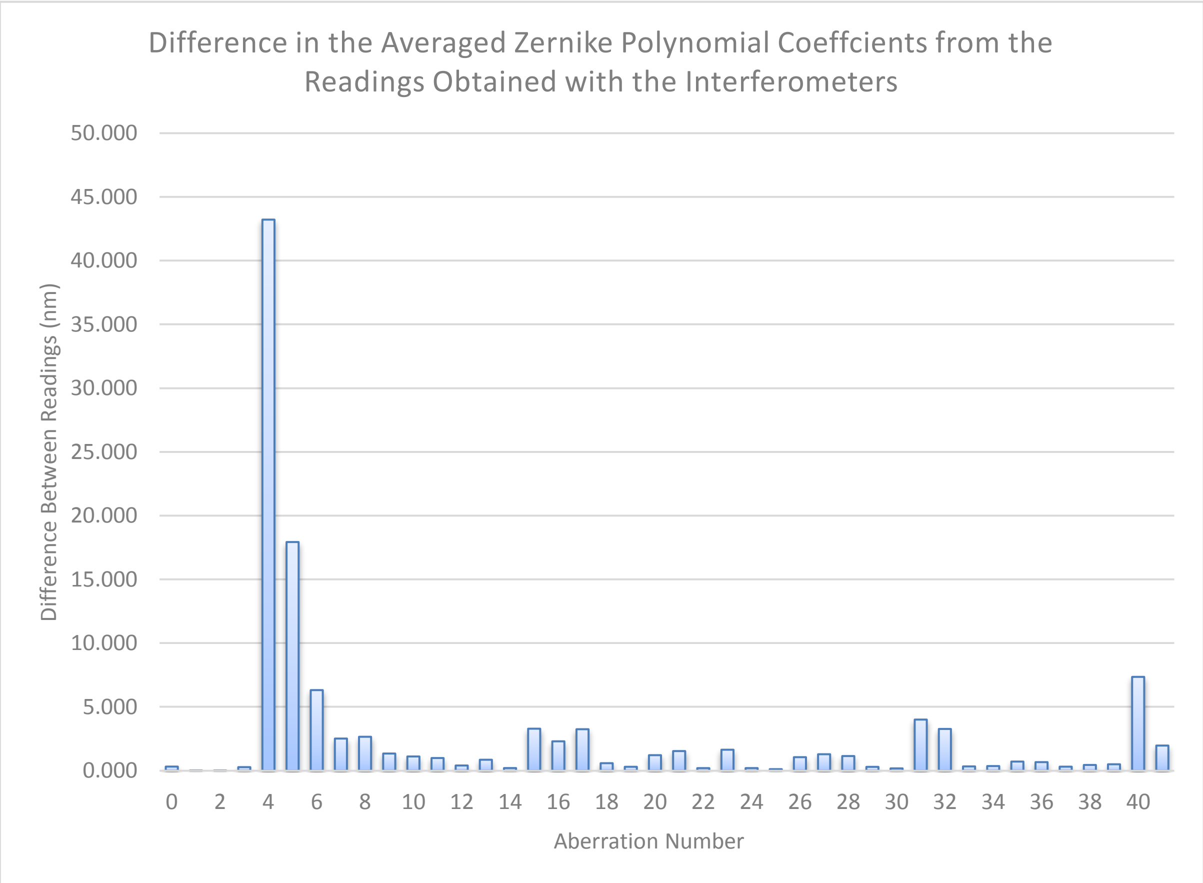

Graph 6: It is apparent that is an inconsistently large measurement difference between the measurements for the 4th and 5th Aberrations. This is discussed in the analysis section and the raw data can be found in Section 11.1.

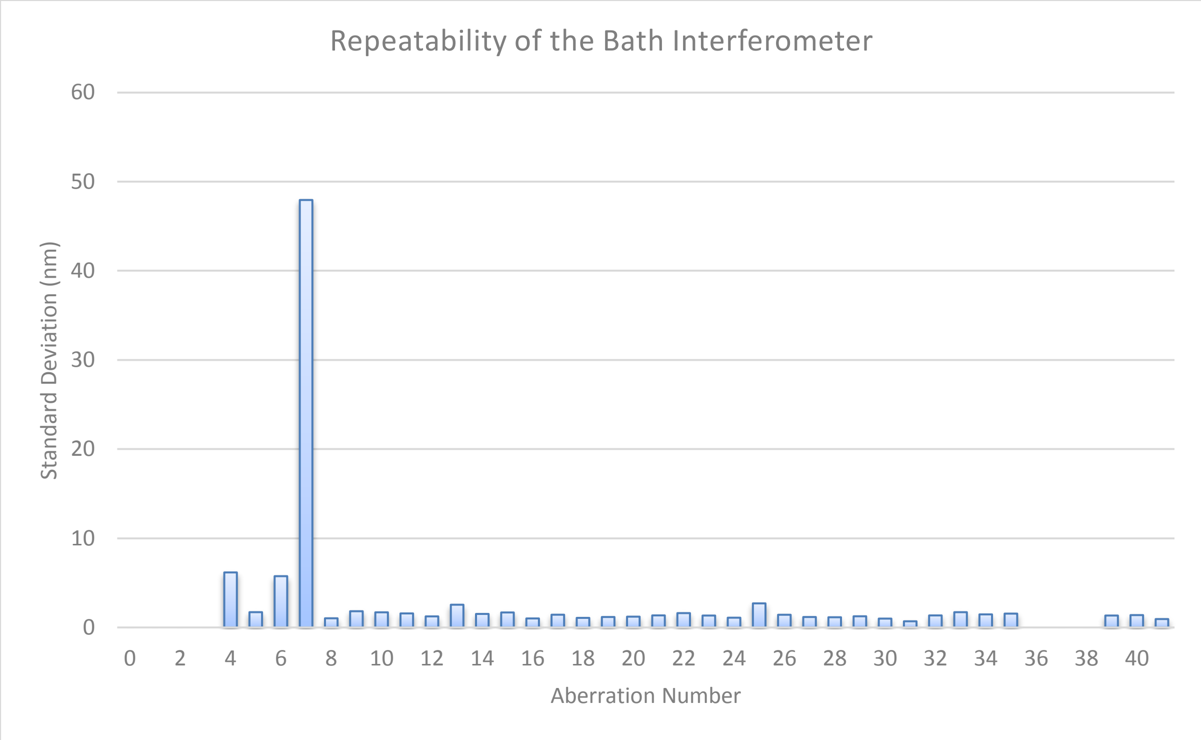

Graph 7: It is apparent that there is an inconsistently large standard deviation value for the 7th Aberrations. This is discussed in the analysis section and the raw data can be found in Section 11.1.2.

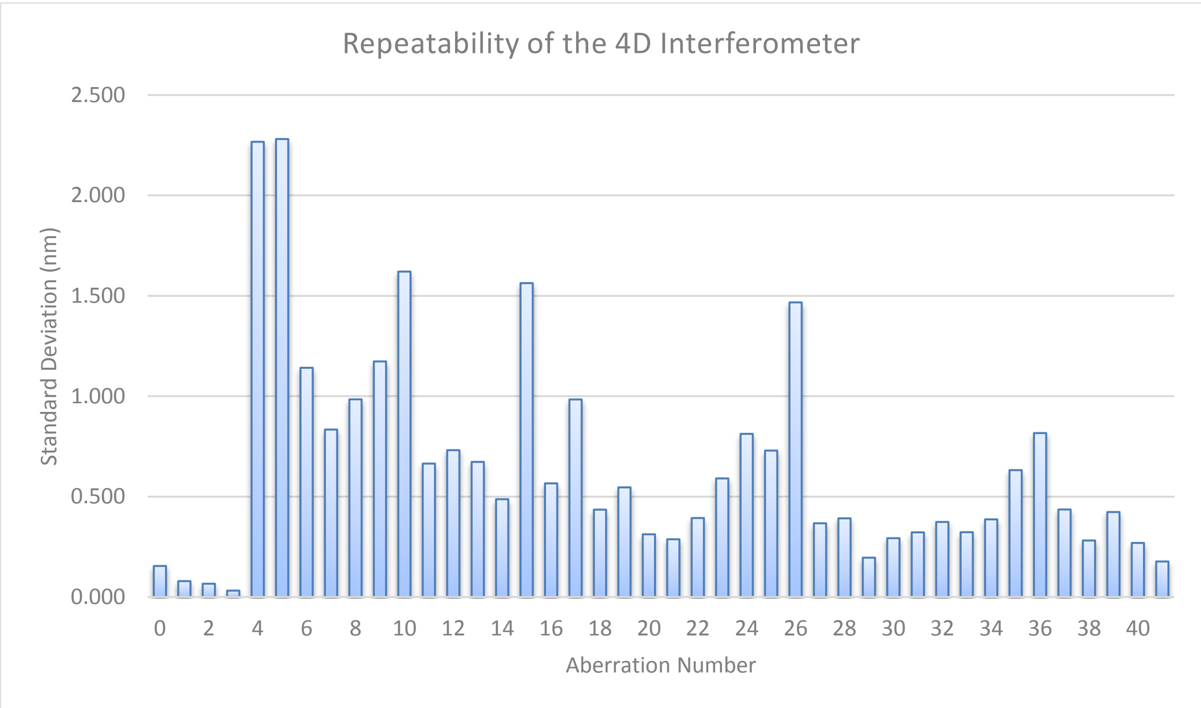

Graph 8: All standard deviation values are under 2.5nm showing the consistency of the 4D interferometer. The raw data can be found in Section 11.1.1.

5.2 200mm Diameter Coated Spherical Mirror

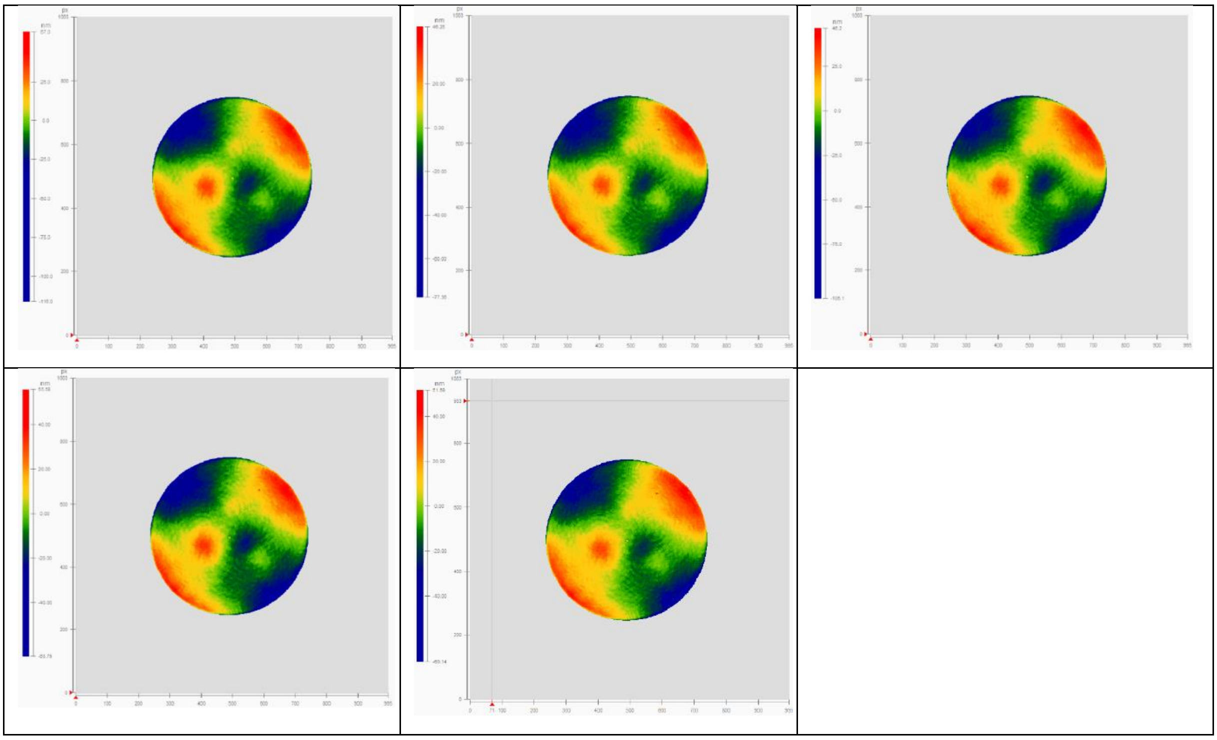

Figure 34: Surface readings obtained with the 4D interferometer of the 200mm spherical mirror. The RMS value of each set is represented by in Table 5 and the Zernike coefficient values can be found in Section 11.2.1.

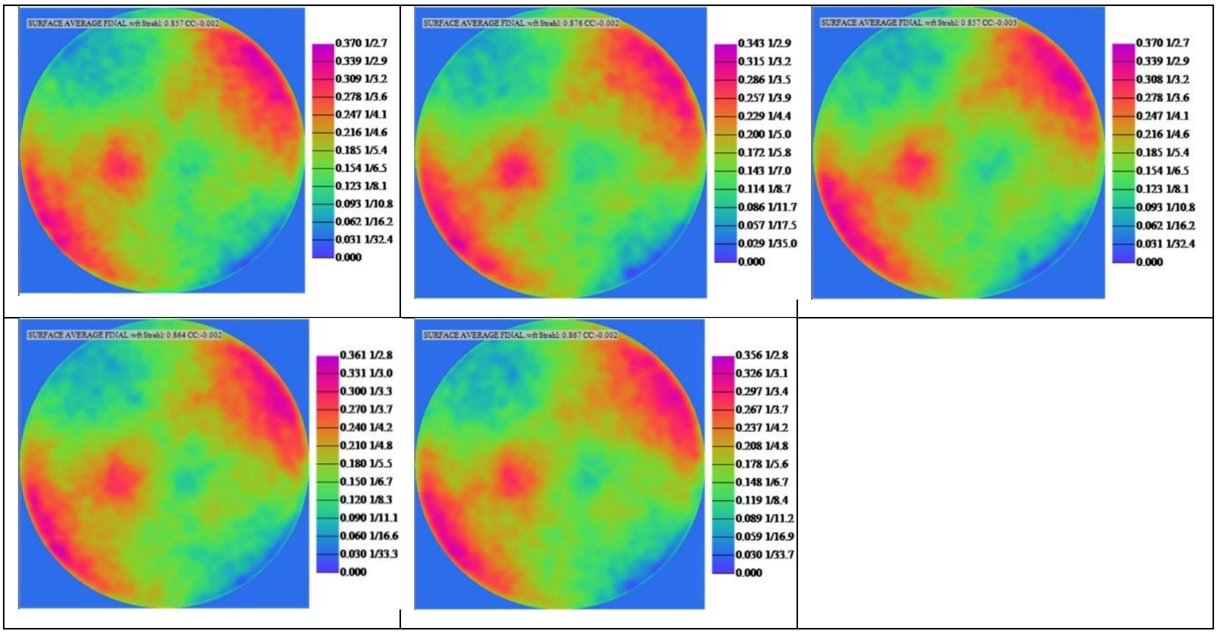

Figure 35: Surface readings obtained with the Bath interferometer of the 200mm spherical mirror. The RMS value of each set is represented by in Table 4 and the Zernike coefficient values can be found in Section 11.2.2.

Table 4 - RMS values obtained for each set with each interferometer

Set	RMS Value obtained with the Bath (nm)	RMS Value obtained with the 4D (nm)
1	17.19	17.58
2	15.99	16
3	17.19	17.67
4	16.77	15.92
5	16.57	17.58
Average	16.74	16.95

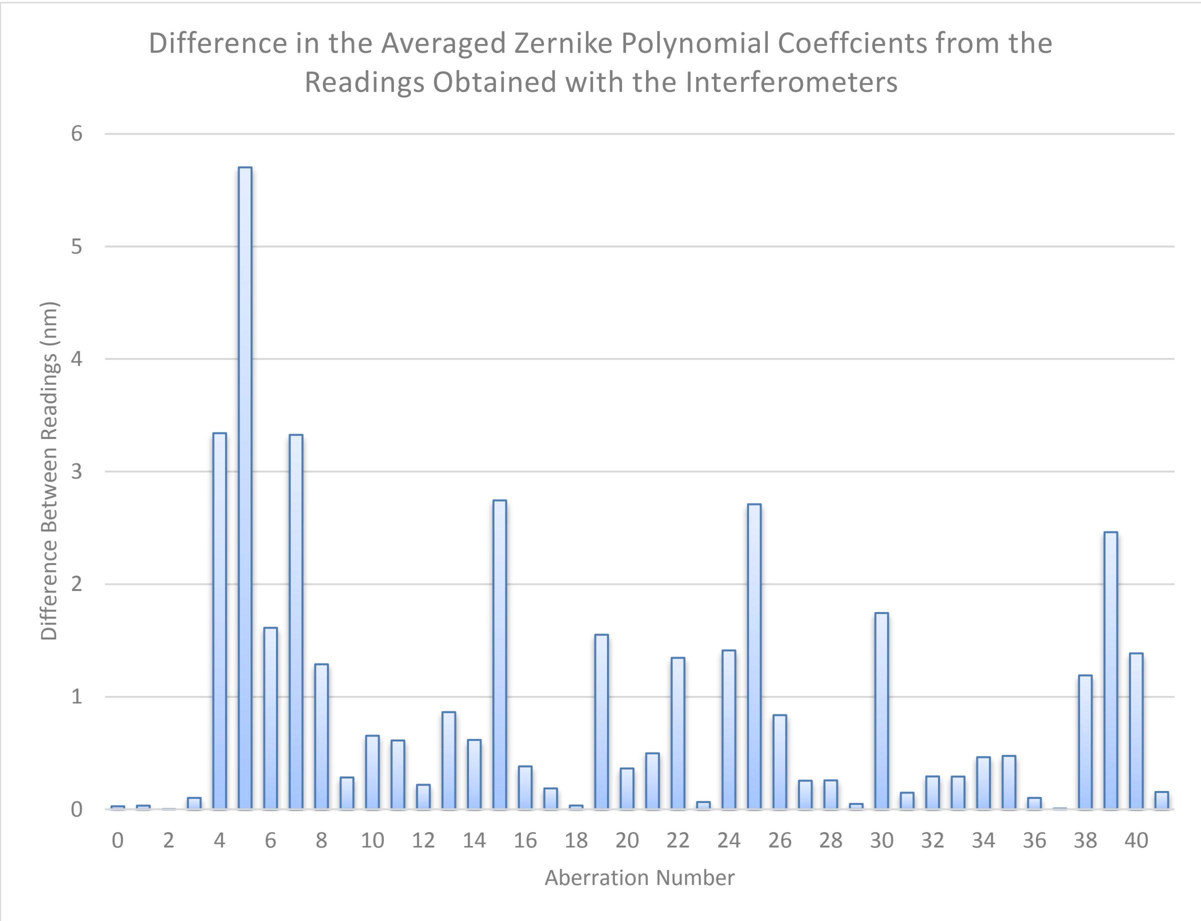

Graph 9: The difference in data obtained from the two interferometers for the 200mm test piece if far superior than the results obtained for the 203mm test piece. The raw data can be found in Section 11.2.

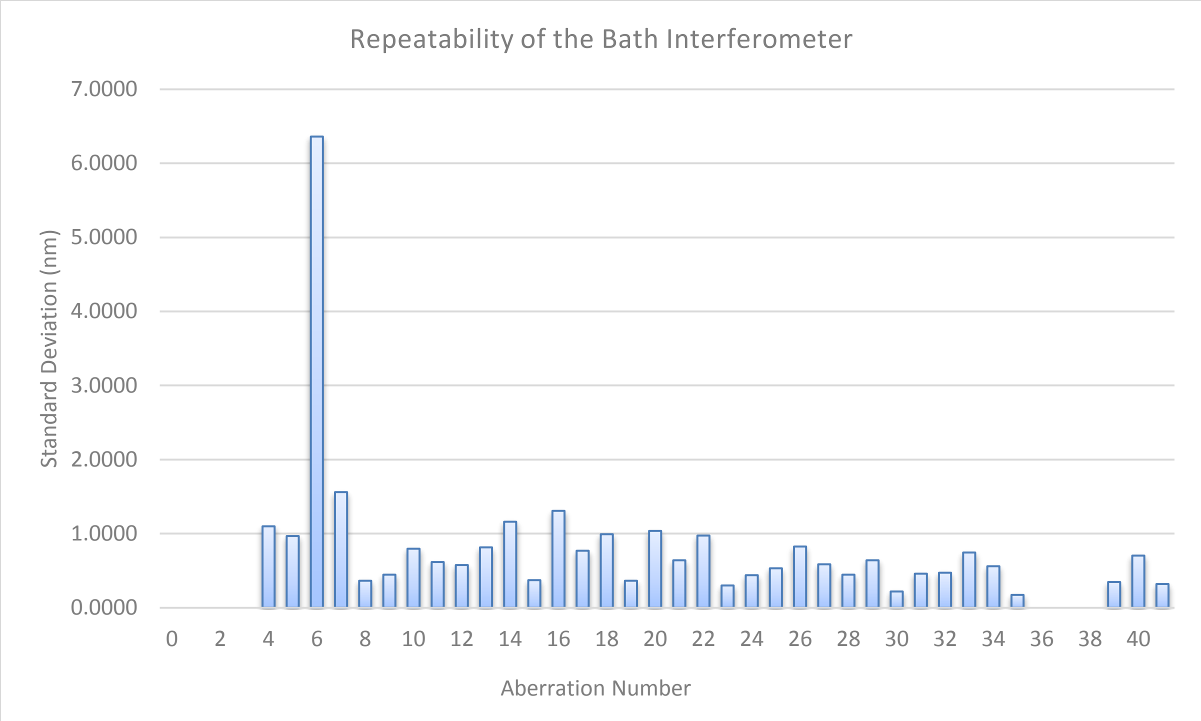

Graph 10: It is apparent that there is an inconsistently large standard deviation value for the 6th Aberration. This is discussed in the analysis section and the raw data can be found in Section 11.2.2.

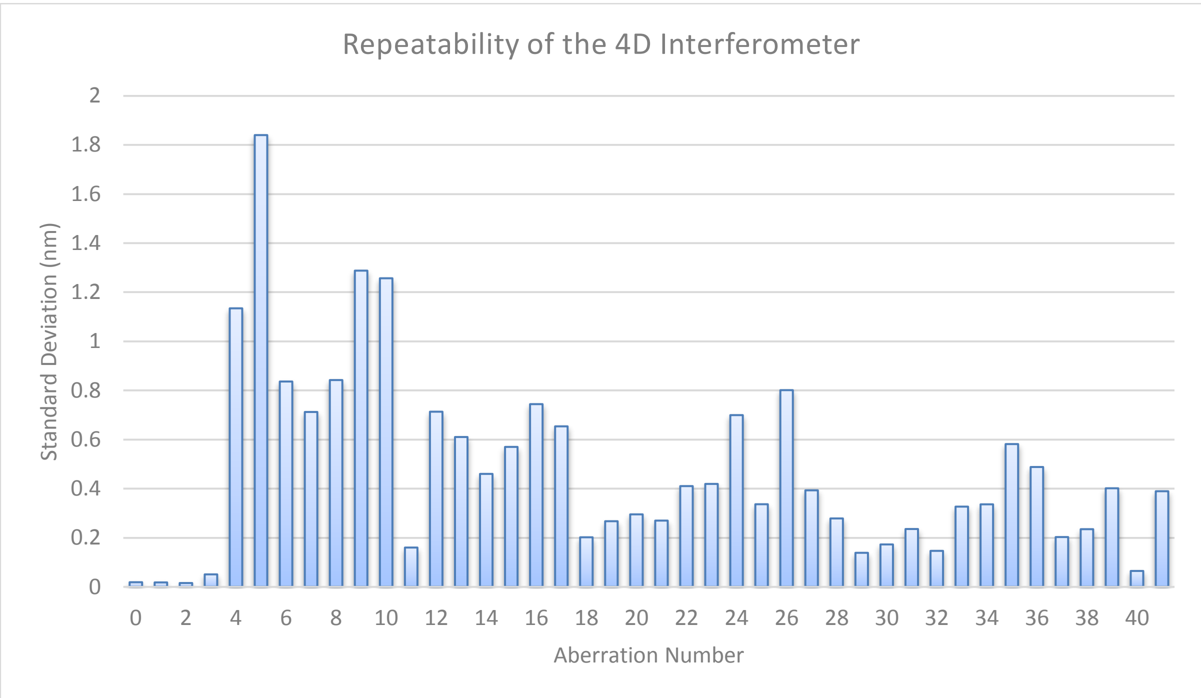

Graph 11: All standard deviation values are under 2nm for the 200mm test piece showing the consistency of the 4D interferometer. The raw data can be found in Section 11.2.1.

5.3 Environmental Susceptibility

Table 5 - RMS values obtained for both sets of data

Single Frame	RMS Value obtained with the Bath without shroud (nm)	RMS Value obtained with the Bath with shroud (nm)
1	24.19	22.96
2	23.20	21.43
3	22.73	22.73
4	23.20	19.74
5	22.50	21.43
6	22.96	19.40
7	23.44	18.60
8	23.44	20.64
9	22.96	19.91
10	23.20	17.44
Average	23.18	20.43

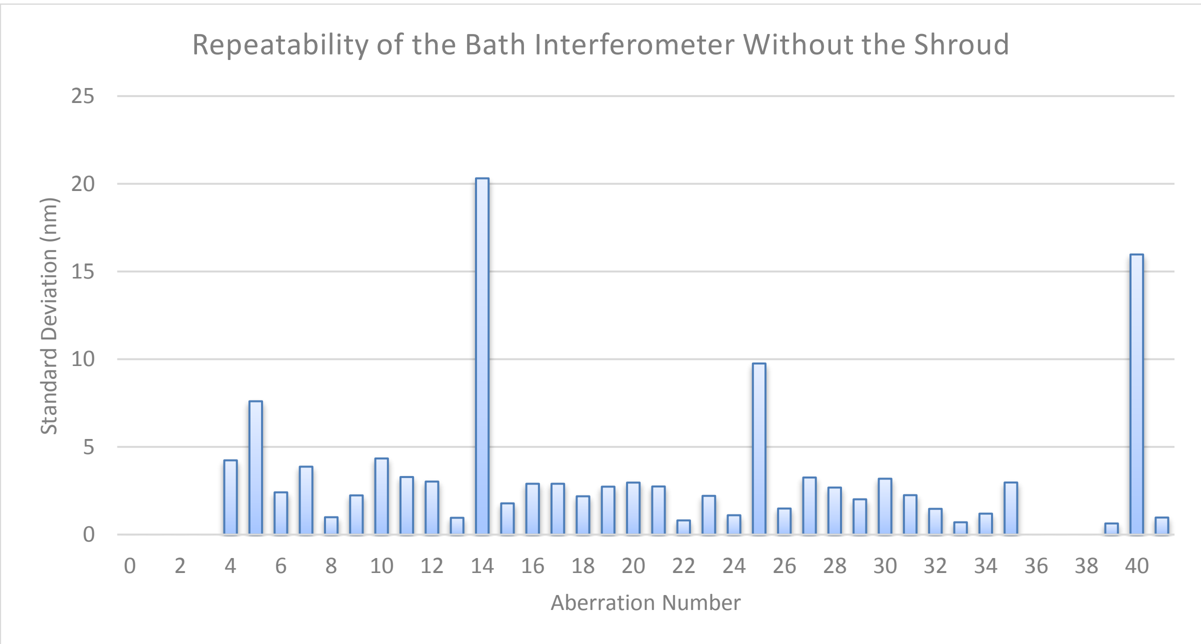

Graph 12: It is apparent that there is an inconsistently large standard deviation value for the 14th and 40th Aberrations. This is discussed in the analysis section.

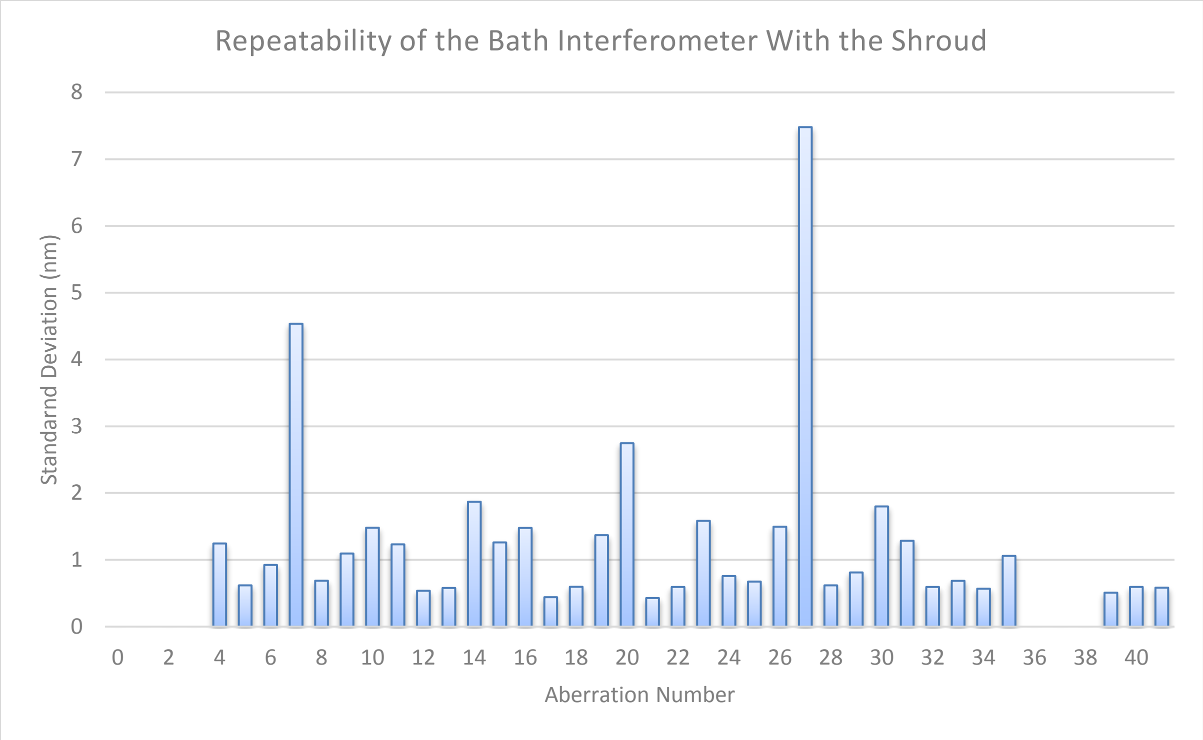

Graph 13: It is clear that the average standard deviation is much lower when the apparatus is protected from thermal air currents. This is further investigated in the analysis section.

6. Analysis

6.1 Analysis of Readings Obtained from the Test Pieces

6.1.1 203mm Diameter Uncoated Spherical Mirror

Both interferometers showed that the 203mm diameter test piece had major astigmatism associated with it. This occurred both visually (Figure 32 & 33) and statistically (refer to Section 11.1). Although both interferometers visually produced a surface with the same form, a more in-depth analysis is required. Statistically analysing the data provides a greater insight into the interferometers performance. Both interferometers consistently produced comparable RMS values (Table 3) and there was a 2.94 ±2.22 nm difference between the averaged RMS values obtained from the two interferometers. This is a difference of 2.5% of the calculated RMS values which was 117.05 ±2.22 nm. Therefore when only considering the visual and RMS results, the two interferometers perform similarly.

When the Zernike polynomials are considered, the two interferometers produce dissimilar results, more specifically the coefficient value of the primary astigmatism in the 203mm diameter test piece. When referring to Graph 6, it is unusual that once the sets have been averaged and compared, there is a difference of 43.23 ±6.57 nm in the astigmatism X coefficient (Aberration number 4) and a 17.94 ±2.85 nm difference in the astigmatism Y coefficient (Aberration number 5) between the results obtained with the interferometers. These two values are much greater than the other Zernike coefficient differences, with the mean difference being 2.79 ±2.92 nm. This difference is unlikely due to environmental effects as the standard deviation for the primary X & Y astigmatism coefficients obtained from the Bath interferometer are 6.16 nm and 1.7 nm respectively (Graph 7). The deviation in the primary X astigmatism is much larger than the mean deviation, which is 2.84 ±7.51 nm (refer to Section 11.1.2) meaning that this deviation due to environmental effects could be the source. As mentioned, the mean standard deviation across the Zernike coefficients is 2.84±7.51 nm, demonstrating consistency in the results obtained by the Bath interferometer.

Curiously, the largest contribution to the mean deviation is from coma X (Aberration number 7). This optical part is meant to be spherical meaning there should not be any coma present in the optic. This value for deviation is almost 10x larger than any other value. The data from the 4D shows that the 203nm diameter optic has values of -1.90 ±1.14 nm and 9.44 ±0.83 nm for Coma X & Y respectively (refer to Section 11.1.1). From the results the optic appears not to be spherical as first thought. This means that the large deviation of coma X in the results from Bath could be attributed to miss alignment. When excluding Coma X from the results it is clear that the repeatability of the Bath interferometer is very good with the mean deviation dropping to 1.54 ±1.19 nm. The repeatability of the 4D as shown in Graph 8 is excellent as expected, with the mean deviation being 0.74 ±0.51 nm.

The reason why there is such a large different in the coefficient values of primary X & Y astigmatism still needs to be uncovered. It is well documented **[1]** that the Bath interferometer has inherent astigmatism associated with its design which could be a contributing factor, although the astigmatism added by the interferometer should have been removed as a result of surface rotations. It is possible that there could be some instrument induced astigmatism left in the readings that was not fully removed. To gain a better insight into this irregularity, the results obtained from the 200mm diameter test piece need to be referred. The readings for the 200mm diameter test piece show that the difference in the primary X & Y astigmatism are both under 3.34 ±1.58 nm & 5.70 ±2.08 nm (Graph 9), which is a large improvement. This comparison would suggest that the inherent astigmatism of the Bath interferometer is not the cause of the large difference in the readings obtained of primary X & Y astigmatism for the 203mm diameter test piece. This information would suggest that either the Bath interferometer or the software has limitations in obtaining accurate values for primary X & Y astigmatism in optics with large coefficients for these Zernike polynomials. To accurately determine the source of this deviation, further testing is required into optics with large astigmatism and into the analysis tool (OpenFringe). Of course, this is all assuming that the data from the 4D interferometer are the correct results which could be an incorrect assumption, but considering the Bath interferometer has problems with astigmatism, it is likely the source of the difference.

Although the results for the comparison of primary X & Y astigmatism raises concern, the Bath interferometer compared to the 4D interferometer fairly well in terms of repeatability (Graph 7 & 8) and results, both visually and statistically. Most Zernike coefficients were in comparable range and the average surface RMS values of 115.58 ±1.99 nm for the Bath and 118.52 ±0.98 nm for the 4D interferometers were both comparable and consistently produced. These results are extremely promising when you consider the price difference of the two interferometers (£121.40 for the Bath interferometer and £140,000 for the 4D 6000 interferometer), although this difference in the primary astigmatism does raise concern.

6.1.2 200mm Diameter Coated Spherical Mirror

The 200mm diameter test piece has a much more distinctive surface structure with the aberrations not being overwhelmed by a singular aberration. Visually, both interferometers consistently produced similar surface structures with the key features being present in every contour map (Figure 34 & 35) and when considering the statistics, the results are just as comparable. The Bath interferometer calculated the surface RMS to be 16.74 ±0.45 nm whilst the 4D interferometer calculated it to be 16.95 ±0.80 nm, these results are promisingly similar. The difference between the averaged Zernike coefficients obtained from the two interferometers has a mean value of 0.95 ±1.20 nm (Graph 9). Once again the largest difference in an Aberration was in the primary X & Y astigmatism, though this is nowhere near the scale in the 203mm diameter test piece. Results from both interferometers produced a difference of 3.34 ±1.58 nm and 5.7±2.08 nm in the primary X & Y astigmatism respectively (Graph 9). Considering the Bath interferometer reportedly has issues with astigmatism, these results are positive. These results are supported when you consider the averaged Zernike polynomials difference is only 0.95 ±1.20 nm (Graph 9) and an averaged RMS difference of 0.21 ±0.92nm (Table 4).

The repeatability of the Bath interferometer for this test piece is outstanding with the standard deviation taking mean value of 0.78 ±0.98 nm (Graph 10). Much like the results for test piece 1, the largest standard deviation values were for coma X & Y, taking values of 6.63nm and 1.56 respectively. Although this test piece is meant to be spherical, the 4D interferometer provided values of 4.42 ±0.84 nm and -1.30 ±0.71 nm for average coma X & Y respectively (refer to Section 11.2.1). Therefore the 200mm diameter mirror is not perfectly spherical, meaning that the large value for standard deviation can be attributed to miss alignment. These results provide an insight into Bath interferometer technological capabilities. The repeatability of the 4D interferometer was once again extremely good with a standard deviation mean of 0.53 ±0.40nm, which is only slightly superior to the results obtained by the Bath interferometer.

The results obtained from the 200mm diameter test piece demonstrate the effectiveness of Bath interferometer. Not only did the Bath interferometer visually match the results from the 4D interferometer, but also matched the statistical values in term of repeatability and final Zernike polynomial values.

6.2 Analysis of Readings Obtained from Changing Environmental Factors

The changing environmental conditions experiment was conducted to obtain an insight into the Bath interferometer susceptibility to thermal air currents. There was a noticeable difference in the results when the apparatus was protected against thermal air current to when it was exposed.

When the experiment was exposed to thermal air currents, the average standard deviation across all the polynomials is 3.27 ±4.00 nm (Graph 12). This value is 6x larger than the results from the multiple frame experiment (Graph 10). The surface RMS values were consistently in the vicinity of 23 nm, leading to an averaged value of 23.18 ±0.44 nm (Table 5). This value is 6.44 ±0.62 nm larger than the surface error that was previously calculated, a considerable difference. The visual results, although they vary from reading to reading, still contain some of the key points of the surface. These result were to be expected as it is well documented that if thermal air currents are not managed, they will cause inconsistent results.

The readings obtained with the Bath interferometer when protected against thermal air currents revealed noticeable improvement. The average standard deviation across all the polynomials dropped to 1.18 ±1.30 nm (Graph 13), this is a third of when the apparatus was unprotected. The averaged RMS value obtained was 20.43 ±1.67 nm (Table 5), an improvement but still considerably different than the calculated value. Visually is where the largest improvement occurs, across all 10 readings, the surface maintained a consistent shape with all the key features clearly visible. These results suggest that although there are benefits to protecting the test from thermal air currents, multiple frame averaging will average out environmental effects meaning protection isn't a necessity.

Although an insight into the environmental sensitivity was obtained, due to the nature of the experiment no conclusions can be drawn as a larger set of data is required for conclusive results. But these results do underline the importance of frame averaging and how imperative it is to average out environmental effects.

7. Conclusion & Future Research

The experiments that have been conducted in this report have further shown that the Bath interferometer is a technology with great capability and potential. It has proved itself when compared to one of the industry's leading interferometers in terms of visual and statistical accuracy. This being said, there are still multiple issues that require investigation such as the ability to accurately measure an optic with large amounts of astigmatism. In order to confirm whether the Bath design does have an issue with accurately measuring optics with large amounts of astigmatism, an experiment needs to be conducted on multiple optics, all containing primary astigmatism coefficients of at least 150nm. It would also be prudent to rotate the optic so that the 0° lies directly over the largest astigmatism component and then 90° to this component allowing the optic to be tested when primary X astigmatism is large and then when primary Y astigmatism large. The data should then be analysed with 4Sight in order to rule out the possibility of OpenFringe causing the error. With these test conducted, a further insight into this issue should be attained and could lead to the issue being resolved or become accounted for.

Component quality is another area that requires further research. It is important to remember that the Bath interferometer prototype used in this experiment cost £120 to construct, which could potentially be reduced to £30. Although the Bath interferometer prototype performed extremely well, there is still room for improvement. With a calibrated light source and a high quality bi-convex lens, measurements could become more accurate. But the question that needs answering is by how much will the accuracy improve? And does the increase accuracy warrant the price increase? It is important not to forget that the purpose of this experiment in to uncover an interferometer that has a high performance but is also of low cost. By unnecessarily increasing production cost could put the Bath interferometer over the consumer's budget. But if a components is upgraded and leads to noticeable accuracy improvement for a low cost, the replacement could be worth considering. But with all things considered, the current components being implemented have proved to be very effective.

The software OpenFringe proved to be extremely user friendly with some very practical features. Interferogram analysis can be done swiftly and effectively as shown in the results. The files for the analysed data can be easily converted into a surface map allowing for the data to be imputed into software packages for mechanical polishing tools, MATLAB or even other interferometer software's such as 4Sight.

So in conclusion, Bath interferometer has proven to be an extremely capable technology and most definitely has the potential to enter the market as a low cost, highly accurate and reliable interferometer.

9. References

[1] Scherman, Michael S. (2012). **Laser Interferometry of Parabolic Newtonian Telescope Mirrors with a Bath Interferometer and Analysis of Wavefront and Figure in OpenFringe.** Unpublished work.

[2] Matt Novak and James C. Wyant. **Dynamic Interferometry**. Proc. of SPIE Vol. 5875

[3] Malacara, Daniel, ed. ***Optical shop testing***. Vol. 59. John Wiley & Sons, 2007.

[4] Shankland, Robert S. **Michelson-Morley Experiment**. *American Journal of Physics* 32.1 (1964): 16-35.

[5] Carnal, Olivier, and Jürgen Mlynek. **Young's double-slit experiment with atoms: A simple atom interferometer**. *Physical review letters* 66.21 (1991): 2689.

[6] Wyant, James C. (1992). **Basic Wavefront Aberration Theory for Optical Metrology. In: Wyant, James C.** ***APPLIED OPTICS AND OPTICAL ENGINEERING, VOL. XI***. Arizona: Academic Press, Inc. 1-53.

[7] Rowe, David. **FringeXP: A Fringe Analysis Program**, Ver. 2. (2003).

[8] Saif, Babak N., et al. **Instantaneous phase-shifted speckle interferometer for measurement of large optical structures**. *Astronomical Telescopes and Instrumentation*. International Society for Optics and Photonics, 2004.

[9] Creath, K., **Phase measurement interferometry techniques**. Progress in Optics. **26** 349-393 (1988).

[10] Eso News. (2014). ***Another world-first for scientists in telescope race.*** Available: http://www.glyndwr.ac.uk/en/AboutGlyndwrUniversity/Newsandmediacentre/Newsarchive/PressReleases2014/ESOnews/. Last accessed 02.12.2014.

[11] Hellemans, Alexander; Bryan Bunch (1988). ***The Timetables of Science***. New York City: Simon and Schuster. 317.

[12] Earl R. Hoover (1977). ***Cradle of Greatness: National and World Achievements of Ohio's Western Reserve***. Cleveland: Shaker Savings Association. 20.

[13] Wyant, James C. (1992). **Basic Wavefront Aberration Theory for Optical Metrology. In: Wyant, James C.** ***APPLIED OPTICS AND OPTICAL ENGINEERING, VOL. XI***. Arizona: Academic Press, Inc. 1-53.

[14] Malacara, Daniel. (2007). **Polarizing Cube Beam Splitter**. In: Malacara, Daniel *Optical Shop Testing*. 3rd ed. New York: A John Wiley & Sons, Inc.. 46-70.

[15] Tomasz J. Licznerski ; Henryk T. Kasprzak ; Waldemar Kowalik. (1999). **Application of Twyman–Green Interferometer for Evaluation of In Vivo Breakup Characteristic of the Human Tear Film**. *J. Biomed. Opt.* 4 (1), 176-182.

[16] Podbielska, Halina Ewa. (1996). **High precision Twyman-Green interferometer for the measurement of ophthalmic surfaces**. *Acta Ophthalmologica Scandinavica*. 74 (4), 348-353.

[17] Goldstein, R J. (1965). **Interferometer for Aerodynamic and Heat Transfer Measurements**. *AIP*. 36 (1), 1408.

[18] Ristić, Slavica. (2012). **Flow visualization techniques in wind tunnels – optical methods (Part II)**. *Military Technical Institute*. 1 (1), 38-49.

[19] Dohlen, K.. (2004). **Phase masks in astronomy: From the Mach-Zehnder interferometer to coronagraphs**. *EAS Publications Series*. 12 (1), 33-44.

[20] Gerry, Christopher C. (1999). **Generation of optical macroscopic quantum superposition states via state reduction with a Mach-Zehnder interferometer containing a Kerr medium.** *Phys. Rev*. 59 (1), 40-95.

[21] Heideman, R.G. ; Lambeck, P.V.. (1999). **Remote opto-chemical sensing with extreme sensitivity: design, fabrication and performance of a pigtailed integrated optical phase-modulated Mach–Zehnder interferometer system**. *Sensors and Actuators B: Chemical*. 61 (1-3), 100-127.

[22] Min Xiao ; Yong-qing Li ; Shao-zheng Jin ; Julio Gea-Banacloche. (1995). **Measurement of Dispersive Properties of Electromagnetically Induced Transparency in Rubidium Atoms**. *Phys. Rev*. 74 (1), 666.

[23] Malacara, Daniel (1989). ***Physical Optics and Light Measurements***. New York: Academic Press . 43- 150.

[24] BATH, Karl-Ludwig. (1973). **A simple interferometer for testing astronomical optics** . *Sterne und Weltraum*. 6 (1), 177-180.

[25] Scherman, Michael S. (2012). **Laser Interferometry of Parabolic Newtonian Telescope Mirrors with a Bath Interferometer and Analysis of Wavefront and Figure in OpenFringe.** Unpublished work.

[26] Koehler, Stephen C. (2005). **Interferometry Comparison**. Unpublished work.

10. List of Acronyms

Bath - Bath Interferometer

4D - 4D Technology "dynamic" PhaseCam 6000 laser interferometer

4Sight – 4Sight Data Analysis Software

FFT – Fast Fourier Transform

Astig – Astigmatism Aberration

CAD – Computer-Aided Design

QWP – Quarter-Wave Plate

11. Appendices

11.1. Data for 203 Diameter Test Piece

11.1.1. Data Obtained with the 4D Interferometer

		Coefficients for Surface (nm)					
	Aberration	1st	2nd	3rd	4th	5th	6th
0	Piston or Bias	-0.56952	-0.25312	-0.44296	-0.0498	-0.56952	-0.25312
1	Tilt X	-0.0594	-0.12656	0.043	0.0633	0.0633	-0.0319
2	Tilt Y	-0.0633	0.0039	-0.0428	-0.12656	0.12656	-0.0174
3	Power	-0.3164	-0.25312	-0.3164	-0.25312	-0.3164	-0.25312
4	Astig X	179.7	174.8	174.3	173.2	172.1	173.3
5	Astig Y	-229.4	-230.9	-230.1	-228.9	-225.1	-229.8
6	Coma X	-1.392	-2.974	-1.519	-1.076	-2.911	-1.266
7	Coma Y	9.365	8.669	9.429	10.95	9.555	8.733
8	Primary Spherical	-8.226	-9.619	-10.25	-9.682	-6.771	-9.682
9	Trefoil X	8.922	4.683	7.53	5.569	7.214	7.214
10	Trefoil Y	-2.088	-6.012	-2.784	-4.176	-2.341	0.12656
11	Secondary Astig X	-6.708	-5.379	-5.252	-5.948	-6.075	-5.569
12	Secondary Astig Y	12.53	12.91	12.15	14.24	12.09	13.42
13	Secondary Coma X	-0.50624	1.012	0.82264	0.50624	1.266	0.44296
14	Secondary Coma Y	0.44296	-0.12656	0.0633	0.69608	1.392	0.25312
15	Secondary Spherical	-17.15	-17.97	-18.16	-18.54	-13.48	-16.96
16	Tetrafoil X	4.43	5.062	4.493	4.24	4.24	5.758
17	Tetrafoil Y	12.53	13.98	11.58	13.42	13.48	13.35
18	Secondary Trefoil X	-2.468	-2.341	-2.974	-1.266	-2.341	-2.531
19	Secondary Trefoil Y	1.772	1.835	1.076	2.341	1.392	0.9492
20	Tertiary Astig X	-10.25	-10.88	-11.01	-10.5	-10.31	-10.57
21	Tertiary Astig Y	8.48	7.91	7.973	7.783	7.72	8.29
22	Tertiary Coma X	0.44296	-0.6328	0.18984	0.75936	0.6328	0.6328
23	Tertiary Coma Y	-4.746	-4.619	-3.923	-5.252	-3.037	-4.05
24	Tertiary Spherical	-18.6	-18.6	-18.98	-18.6	-16.9	-19.49
25	Pentafoil X	0.6328	-0.12656	0.18984	0.37968	0.37968	-0.25312
26	Pentafoil Y	3.037	4.24	3.037	-0.75936	2.468	3.923
27	Secondary Tetrafoil X	-0.25312	-0.82264	-0.69608	-0.88592	-0.37968	-1.266
28	Secondary Tetrafoil Y	-5.442	-6.201	-4.809	-5.316	-5.189	-6.012

29	Tertiary Trefoil X	-0.12656	0.18984	-0.25312	-0.25312	-0.25312	-0.3164
30	Tertiary Trefoil Y	-0.69608	-0.56952	-0.37968	-0.44296	-0.6328	-0.25312
31	Quaternary Astig X	9.112	8.669	9.239	8.606	8.226	9.112
32	Quaternary Astig Y	-9.619	-9.365	-10.25	-9.619	-9.302	-9.998
33	Quaternary Coma X	-0.6328	-0.0633	-0.82264	-0.9492	0.0086	-0.3164
34	Quaternary Coma Y	0.6328	0.75936	1.329	0.3164	1.266	1.266
35	Quaternary Spherical	-3.164	-3.354	-3.86	-3.797	-2.784	-3.987
36	Hexafoil X	0.75936	-0.12656	0.25312	-1.709	-1.202	-1.772
37	Hexafoil Y	-0.9492	-0.50624	-0.44296	-0.82264	-0.04	-0.44296
38	Secondary Pentafoil X	-0.44296	-0.56952	-0.44296	-0.9492	-0.3164	-0.3164
39	Secondary Pentafoil Y	-2.215	-3.101	-2.721	-1.645	-2.848	-2.974
40	Tertiary Tetrafoil X	-0.0437	0.25312	0.69608	0.69608	0.50624	0.82264
41	Tertiary Tetrafoil Y	0.75936	1.202	0.88592	0.56952	0.88592	0.88592

Table laterally continued.

Coefficients for Surface (nm)					
7th	8th	9th	10th	Mean (nm)	Standard Deviation(nm)
-0.3164	-0.18984	-0.3164	-0.3164	-0.327708	0.154266
0.0052	-0.12656	0.0026	0.12656	-0.004046	0.0789501
-0.0034	-0.0137	0.0591	0.0427	-0.00349	0.066019
-0.25312	-0.3164	-0.3164	-0.25312	-0.28476	0.03164
176.1	171.5	175.6	176.2	174.68	2.2670686
-229.6	-232.7	-233.7	-227.8	-229.8	2.2807893
-1.709	-1.202	-4.493	-0.44296	-1.898496	1.1414916
9.302	9.492	10.76	8.1	9.4355	0.8338409
-9.112	-9.935	-8.796	-8.416	-9.0489	0.9843249
6.898	7.91	7.973	7.91	7.1823	1.1731933
-0.56952	-2.594	-2.278	-2.088	-2.480396	1.6207527
-7.151	-4.999	-5.126	-6.012	-5.8219	0.6643888
12.66	11.77	12.4	11.77	12.594	0.7312072
1.202	0.0289	1.519	1.835	0.81285	0.6727096
0.18984	0.56952	0.88592	1.329	0.569518	0.4868756
-19.24	-18.22	-19.17	-17.66	-17.655	1.5631011
3.67	4.683	4.366	5.252	4.6194	0.5658482
13.98	14.24	12.02	14.93	13.351	0.983783
-1.772	-2.405	-2.278	-2.341	-2.2717	0.4350108
1.012	1.582	1.012	0.3164	1.32876	0.5458022
-10.19	-10.5	-10.38	-11.14	-10.573	0.3122195
8.163	8.606	8.353	8.353	8.1631	0.2873717

0.25312	-0.0633	0.0056	0.37968	0.260006	0.3932457
-4.556	-4.24	-3.67	-3.987	-4.208	0.5904358
-19.68	-19.05	-20.06	-18.86	-18.882	0.8123645
-0.6328	1.266	2.025	0.69608	0.45566	0.7291749
1.645	2.088	0.37968	1.455	2.151332	1.4671938
-0.69608	-1.455	-0.75936	-1.266	-0.847988	0.3670423
-5.442	-5.822	-5.252	-5.505	-5.499	0.3916036
-0.12656	-0.12656	-0.18984	0.3164	-0.113904	0.195657
-0.25312	-0.12656	-0.37968	0.37968	-0.335384	0.2928025
8.796	9.049	9.049	8.416	8.8274	0.3218149
-9.935	-10.06	-10.57	-9.808	-9.8526	0.3735741
-0.18984	-0.6328	-0.3164	-0.0633	-0.397808	0.3225557
0.56952	1.202	1.582	1.139	1.006208	0.3864689
-4.556	-4.43	-4.873	-3.354	-3.8159	0.631696
-1.329	-1.076	-0.25312	-0.3164	-0.67716	0.8163898
0.50624	-0.44296	0.3164	-0.37968	-0.3204	0.4356857
0.0633	-0.25312	-0.44296	-0.88592	-0.455614	0.2812973
-2.848	-2.594	-2.341	-2.974	-2.6261	0.4229606
0.56952	0.69608	0.56952	0.12656	0.489214	0.269072
0.75936	0.56952	0.75936	0.9492	0.822608	0.1766627

11.1.2. Data Obtained with the Bath Interferometer

		Coefficients for Surface (nm)					
	Aberration	1st	2nd	3rd	4th	5th	6th
0	Piston or Bias	0.00	0.00	0.00	0.00	0.00	0.00
1	Tilt X	0.00	0.00	0.00	0.00	0.00	0.00
2	Tilt Y	0.00	0.00	0.00	0.00	0.00	0.00
3	Power or Defocus	0.00	0.00	0.00	0.00	0.00	0.00
4	Astig X	140.25	145.20	130.63	124.03	129.53	131.18
5	Astig Y	-213.68	-207.90	-213.13	-210.10	-213.95	-211.75
6	Coma X	12.65	0.83	0.28	-3.85	4.68	3.03
7	Coma Y	-64.35	138.33	8.53	-1.65	-13.75	6.33
8	Primary Spherical	-12.10	-11.28	-9.35	-12.38	-11.55	-12.10
9	Trefoil X	1.65	5.23	6.88	6.88	7.43	8.25
10	Trefoil Y	-0.83	-7.43	-3.03	-4.68	-2.75	-4.13
11	Secondary Astig X	-10.45	-7.70	-6.33	-6.60	-6.60	-5.78
12	Secondary Astig Y	10.45	13.75	12.93	13.20	12.38	15.40
13	Secondary Coma X	1.38	-1.93	3.30	0.55	-0.28	2.75
14	Secondary Coma Y	-1.10	-0.83	-0.28	1.38	1.38	-3.03
15	Secondary Spherical	-23.93	-20.08	-18.70	-21.18	-21.45	-20.35
16	Tetrafoil X	6.05	7.43	6.33	5.78	5.78	6.33
17	Tetrafoil Y	6.60	10.45	10.73	9.63	11.28	8.53
18	Secondary Trefoil X	-2.75	-2.20	-0.55	-0.83	-1.10	0.00
19	Secondary Trefoil Y	0.28	1.10	1.10	1.38	0.55	2.48
20	Tertiary Astig X	-6.60	-8.80	-10.18	-9.35	-9.90	-11.28
21	Tertiary Astig Y	10.73	11.55	11.28	8.80	9.08	10.18
22	Tertiary Coma X	1.38	-3.30	1.65	0.83	-0.28	1.93
23	Tertiary Coma Y	-4.13	-3.03	-2.75	-1.93	-1.93	-5.23
24	Tertiary Spherical	-20.63	-17.88	-16.78	-19.53	-19.25	-18.15
25	Pentafoil X	3.30	4.13	3.03	-2.20	-1.65	-3.03
26	Pentafoil Y	5.23	4.13	1.93	3.58	5.23	2.75
27	Secondary Tetrafoil X	-3.03	-4.13	-0.83	-2.48	-2.48	-2.20
28	Secondary Tetrafoil Y	-4.13	-3.85	-3.58	-3.30	-4.40	-6.88
29	Tertiary Trefoil X	-1.65	0.83	2.20	0.00	0.28	1.65
30	Tertiary Trefoil Y	-0.28	-1.65	0.00	1.38	-0.83	0.00
31	Quaternary Astig X	5.50	4.68	4.40	5.23	4.95	3.58

32	Quaternary Astig Y	-6.60	-3.85	-6.05	-6.60	-7.15	-5.23
33	Quaternary Coma X	2.48	-3.85	0.28	-0.28	-0.28	0.28
34	Quaternary Coma Y	0.83	2.48	-0.55	3.58	1.65	-1.10
35	Quaternary Spherical	-6.88	-4.95	-2.48	-2.48	-4.40	-2.20
36	Hexafoil X	0.00	0.00	0.00	0.00	0.00	0.00
37	Hexafoil Y	0.00	0.00	0.00	0.00	0.00	0.00
38	Secondary Pentafoil X	0.00	0.00	0.00	0.00	0.00	0.00
39	Secondary Pentafoil Y	-4.95	-2.20	-0.83	-4.13	-4.95	-1.93
40	Tertiary Tetrafoil X	-9.08	-7.43	-4.68	-6.88	-7.15	-4.40
41	Tertiary Tetrafoil Y	-2.20	-0.83	-0.28	-2.48	-1.93	0.83

Table laterally continued

Coefficients for Surface (nm)					
7th	8th	9th	10th	Mean (nm)	Standard Deviation (nm)
0	0	0	0	0	0
0	0	0	0	0	0
0	0	0	0	0	0
0	0	0	0	0	0
128.425	125.125	130.9	129.25	131.45	6.1676069
-211.475	-212.025	-212.85	-211.75	-211.86	1.7094297
16.5	2.2	1.65	6.325	4.4275	5.7480263
15.675	21.45	11.275	-2.2	11.9625	0
-12.925	-10.725	-11.825	-12.925	-11.715	1.0230591
4.675	7.15	5.5	4.675	5.83	1.815
-3.85	-4.4	-3.025	-1.925	-3.6025	1.6927585
-4.95	-7.7	-7.425	-4.675	-6.82	1.5691877
12.65	13.2	14.025	12.1	13.0075	1.2362772
7.425	0.55	-0.55	3.575	1.6775	2.5456446
1.65	1.375	1.375	1.65	0.3575	1.5114997
-23.65	-20.35	-18.7	-21.175	-20.955	1.6763726
7.425	7.7	7.425	9.075	6.93	1.0051617
11.55	10.45	10.725	11	10.0925	1.4239053
-2.75	-3.575	-1.375	-1.65	-1.6775	1.0682609
1.375	2.2	1.65	-1.925	1.0175	1.1670502
-8.8	-8.525	-10.175	-9.9	-9.35	1.2049896
7.425	8.25	11	8.8	9.7075	1.3475

2.475	-0.55	-0.55	1.1	0.4675	1.6037476
-0.55	-2.475	-2.75	-0.825	-2.5575	1.3305567
-19.8	-18.425	-17.6	-18.7	-18.6725	1.0892916
-3.85	1.925	1.1	0.55	0.33	2.6966831
1.925	1.1	1.925	4.4	3.2175	1.4185842
-2.475	-0.55	-3.025	-0.275	-2.145	1.1654291
-4.4	-5.775	-2.75	-4.4	-4.345	1.1391773
-1.65	0.55	0.825	-1.1	0.1925	1.2484515
0	-0.55	-0.825	-2.475	-0.5225	0.9873228
6.05	4.4	5.225	4.125	4.8125	0.6875
-8.25	-7.975	-5.775	-8.25	-6.5725	1.3441284
2.2	-1.1	-1.1	0.825	-0.055	1.7076592
1.1	1.1	1.1	3.575	1.375	1.460351
-5.5	-5.5	-4.95	-6.05	-4.5375	1.5471041
0	0	0	0	0	0
0	0	0	0	0	0
0	0	0	0	0	0
-4.125	-3.3	-1.925	-3.025	-3.135	1.331409
-7.975	-7.7	-6.05	-7.425	-6.875	1.380489
-1.65	-1.375	-0.825	-0.825	-1.155	0.935

11.2. Data for 200 Diameter Test Piece

11.2.1. Data Obtained with the 4D Interferometer

		Coefficients for Surface (nm)						
	Aberration	1st	2nd	3rd	4th	5th	Mean (nm)	Standard Deviation (nm)
0	Piston or Bias	-0.06	-0.03	-0.01	-0.02	-0.02	-0.03	0.02
1	Tilt X	-0.06	-0.04	-0.03	-0.02	-0.01	-0.03	0.02
2	Tilt Y	0.01	-0.02	0.00	-0.01	0.02	0.00	0.02
3	Power or Defocus	-0.19	-0.13	-0.06	-0.06	-0.06	-0.10	0.05
4	Astig X	8.61	6.39	5.19	6.58	7.40	6.83	1.13
5	Astig Y	38.73	35.69	39.30	35.06	39.23	37.60	1.84
6	Coma X	5.06	2.91	5.32	4.43	4.37	4.42	0.84
7	Coma Y	-0.70	-0.19	-1.90	-1.77	-1.90	-1.29	0.71
8	Primary Spherical	-1.33	0.02	-2.28	-0.25	-0.44	-0.86	0.84
9	Trefoil X	-1.77	-2.34	1.27	-1.20	-1.96	-1.20	1.29
10	Trefoil Y	0.51	2.22	3.35	1.46	3.99	2.30	1.26
11	Secondary Astig X	-2.34	-1.96	-2.09	-2.03	-2.34	-2.15	0.16
12	Secondary Astig Y	-0.70	0.70	-0.95	-0.63	-1.46	-0.61	0.71
13	Secondary Coma X	-12.53	-11.14	-12.85	-12.40	-11.77	-12.14	0.61
14	Secondary Coma Y	-0.70	-0.95	-0.13	-0.95	0.19	-0.51	0.46
15	Secondary Spherical	-3.35	-1.84	-2.41	-1.77	-2.22	-2.32	0.57
16	Tetrafoil X	1.33	0.25	1.77	0.82	2.41	1.32	0.74
17	Tetrafoil Y	2.15	1.84	0.44	2.28	1.65	1.67	0.65
18	Secondary Trefoil X	4.75	4.81	4.30	4.37	4.49	4.54	0.20
19	Secondary Trefoil Y	3.80	3.61	4.11	3.67	3.29	3.70	0.27
20	Tertiary Astig X	1.71	2.03	1.33	2.09	2.09	1.85	0.30
21	Tertiary Astig Y	2.34	1.65	1.96	1.90	2.34	2.04	0.27
22	Tertiary Coma X	7.34	6.90	7.28	7.09	8.10	7.34	0.41
23	Tertiary Coma Y	-1.27	-1.65	-1.27	-1.27	-0.38	-1.16	0.42
24	Tertiary Spherical	-7.78	-6.08	-7.47	-6.33	-6.27	-6.78	0.70
25	Pentafoil X	-2.34	-2.41	-2.66	-2.72	-1.77	-2.38	0.34
26	Pentafoil Y	0.44	-1.08	-0.63	-1.90	-1.46	-0.92	0.80
27	Secondary Tetrafoil X	0.19	0.57	0.06	0.19	-0.63	0.08	0.39
28	Secondary Tetrafoil Y	0.32	0.13	0.38	0.13	0.89	0.37	0.28
29	Tertiary Trefoil X	-3.29	-3.29	-3.67	-3.42	-3.42	-3.42	0.14
30	Tertiary Trefoil Y	-4.37	-4.24	-4.43	-4.56	-4.05	-4.33	0.17
31	Quaternary	-1.08	-1.65	-0.95	-1.27	-1.20	-1.23	0.24

	Astig X							
32	Quaternary Astig Y	-2.91	-2.85	-2.85	-3.16	-3.16	-2.99	0.15
33	Quaternary Coma X	-5.06	-4.87	-5.06	-5.25	-4.30	-4.91	0.33
34	Quaternary Coma Y	0.76	0.00	0.63	0.51	1.01	0.58	0.34
35	Quaternary Spherical	-3.92	-2.41	-3.61	-2.59	-2.97	-3.10	0.58
36	Hexafoil X	-0.32	-0.25	0.70	-0.76	0.13	-0.10	0.49
37	Hexafoil Y	-0.32	0.32	-0.03	0.06	0.00	0.01	0.20
38	Secondary Pentafoil X	1.20	1.33	0.76	1.20	1.46	1.19	0.23
39	Secondary Pentafoil Y	-1.90	-0.95	-0.95	-1.01	-0.76	-1.11	0.40
40	Tertiary Tetrafoil X	-0.70	-0.57	-0.57	-0.63	-0.51	-0.59	0.06
41	Tertiary Tetrafoil Y	-0.76	-0.95	-0.38	-0.95	-1.58	-0.92	0.39

11.2.2. Data Obtained with the Bath Interferometer

		Coefficients for Surface (nm)						
	Aberration	1st	2nd	3rd	4th	5th	Mean (nm)	Standard Deviation (nm)
0	Piston or Bias	0.00	0.00	0.00	0.00	0.00	0.00	0.00
1	Tilt X	0.00	0.00	0.00	0.00	0.00	0.00	0.00
2	Tilt Y	0.00	0.00	0.00	0.00	0.00	0.00	0.00
3	Power or Defocus	0.00	0.00	0.00	0.00	0.00	0.00	0.00
4	Astig X	11.00	8.53	10.45	11.55	9.35	10.18	1.10
5	Astig Y	33.00	30.25	32.73	31.63	31.90	31.90	0.97
6	Coma X	9.90	-5.50	10.18	-2.48	1.93	2.81	6.36
7	Coma Y	2.75	-0.83	3.03	1.65	3.58	2.04	1.56
8	Primary Spherical	-2.20	-2.20	-2.75	-1.93	-1.65	-2.15	0.36
9	Trefoil X	-2.20	-0.83	-1.65	-1.38	-1.38	-1.49	0.45
10	Trefoil Y	2.48	1.10	1.10	2.75	0.83	1.65	0.80
11	Secondary Astig X	-2.20	-1.65	-0.83	-2.20	-0.83	-1.54	0.62
12	Secondary Astig Y	-0.83	-1.38	0.28	-1.10	-1.10	-0.83	0.58
13	Secondary Coma X	-12.10	-11.55	-12.10	-10.18	-10.45	-11.28	0.82
14	Secondary Coma Y	0.55	-0.83	2.20	-0.83	-0.55	0.11	1.16
15	Secondary Spherical	-5.23	-5.23	-5.50	-4.40	-4.95	-5.06	0.37
16	Tetrafoil X	0.55	2.48	-1.38	1.65	1.38	0.94	1.31
17	Tetrafoil Y	0.83	0.55	1.65	2.75	1.65	1.49	0.77

18	Secondary Trefoil X	3.03	4.40	6.05	4.13	4.95	4.51	0.99
19	Secondary Trefoil Y	1.65	2.20	2.75	1.93	2.20	2.15	0.36
20	Tertiary Astig X	2.75	1.10	1.65	2.20	-0.28	1.49	1.04
21	Tertiary Astig Y	2.20	1.65	0.55	2.20	1.10	1.54	0.64
22	Tertiary Coma X	4.40	6.05	7.43	6.33	5.78	6.00	0.97
23	Tertiary Coma Y	-1.38	-1.38	-0.55	-1.10	-1.10	-1.10	0.30
24	Tertiary Spherical	-7.70	-7.70	-8.25	-8.80	-8.53	-8.20	0.44
25	Pentafoil X	1.10	0.28	0.28	-0.55	0.55	0.33	0.53
26	Pentafoil Y	-1.65	-2.20	-3.03	-0.55	-1.38	-1.76	0.83
27	Secondary Tetrafoil X	0.00	0.00	1.38	-0.28	0.55	0.33	0.59
28	Secondary Tetrafoil Y	0.55	-0.28	0.55	-0.55	0.28	0.11	0.45
29	Tertiary Trefoil X	-2.48	-3.58	-4.13	-3.03	-4.13	-3.47	0.64
30	Tertiary Trefoil Y	-2.48	-2.75	-2.75	-2.75	-2.20	-2.59	0.22
31	Quaternary Astig X	-0.55	-1.93	-1.38	-1.38	-1.65	-1.38	0.46
32	Quaternary Astig Y	-2.75	-3.58	-2.48	-2.20	-2.48	-2.70	0.47
33	Quaternary Coma X	-6.05	-4.40	-4.40	-4.40	-3.85	-4.62	0.75
34	Quaternary Coma Y	0.83	0.28	1.93	0.83	1.38	1.05	0.56
35	Quaternary Spherical	-3.85	-3.58	-3.58	-3.30	-3.58	-3.58	0.17
36	Hexafoil X	0.00	0.00	0.00	0.00	0.00	0.00	0.00
37	Hexafoil Y	0.00	0.00	0.00	0.00	0.00	0.00	0.00
38	Secondary Pentafoil X	0.00	0.00	0.00	0.00	0.00	0.00	0.00
39	Secondary Pentafoil Y	-4.13	-3.58	-3.03	-3.58	-3.58	-3.58	0.35
40	Tertiary Tetrafoil X	-1.93	-1.38	-1.10	-2.48	-3.03	-1.98	0.70
41	Tertiary Tetrafoil Y	-0.83	-1.10	-0.55	-1.10	-0.28	-0.77	0.32

11.3. Literature Review

1.1 Introduction

Interferometry is a technique where, with the use of waves, small displacements, refractive index changes and surface irregularities can be measured to picometre accuracies. Interferometry is a widely used technique and is a vital investigation method in the fields of optical metrology, astronomy, quantum mechanics, nuclear and particle physics, plasma physics, fibre optics, seismology and oceanography along with numerous other fields. The project will be focused in the optical industry and within this field is where the performance of different interferometer technologies will be reviewed. By utilising the superposition of wave's principle it is possible to extract information about an optical surface by analysing the interference of the waves (refer to section 3). Polishers use interferometers regularly to analyse optic parts to determine whether an optic is sufficiently accurate **[1]**. The accuracy required of an interferometer changes from case to case, but generally, the more accurate the interferometer the superior the readings. For example, a house hold mirror does not need to have an RMS value (on average how much the surface deviates from the perfect value. i.e. for a flat mirror, how much the surface deviates from complete flatness.) of 10 nanometres. At the other end of the scale, the work/research currently being conducted by the ESO team of Glyndŵr University St Asaph, requires readings accurate to a few pecometres. In June 2014 they achieved a world first by successfully managing to polish a 1.5 metre optic down to just 7.5 nanometres **[2]** – in context, this equates to the size of a haemoglobin molecule. For projects of that scale specialist equipment is required and not the market that a low budget interferometer is desired. However, vast amounts of amateur astronomers enjoy making their own telescopes and polishing their own optics. This requires access to an accurate interferometer as the more accurate the optic, the better images they will be able to obtain. This is one of the many markets where an affordable, efficient, easily operated and accurate interferometer is desired.

1.2 Interferometry concept

Interferometry utilises the principle of superposition to combine waves in a way where meaningful information can be extracted from the readings. This can be achieved in multiple of ways and over the years many different techniques have been developed to extract information from the interference of waves.

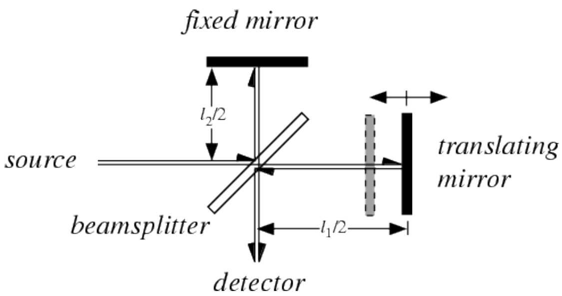

Figure 1: The Michelson interferometer experimental apparatus. Credit: Scienceworld

The Michelson interferometer (Figure 1) is a simple, but extremely effective design and has been involved in some vital experiments over the years - arguably none more important than the Michelson-Morley experiment in 1987 (Refer to section 2.3). The Michelson interferometer is a double path interferometer that produces interference fringes by splitting a beam of monochromatic light into two separate beams with the use of a beam splitter (half-silvered mirror). Each beam has an intensity of 0.5 I_0, with one striking a fixed mirror known as the reference mirror and the other reflecting from the optic under testing mounted on a movable stand. The two beams return along their path and are brought together to produce an interference pattern (Figure 2).

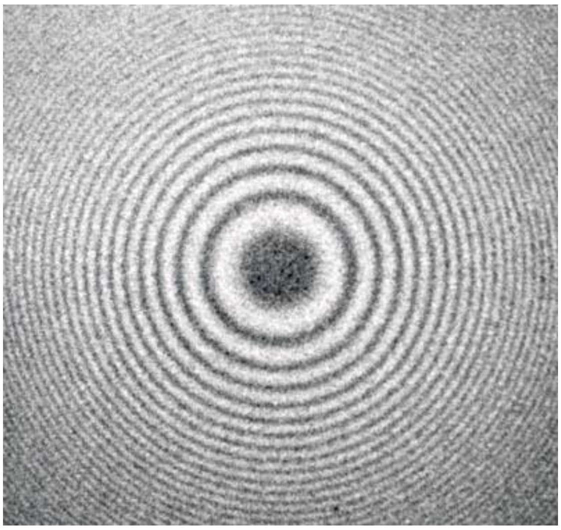

Figure 2: Interference pattern produced from a Michelson Interferometer

By analysing this signal, more specifically conducting Fourier analysis on the interferograms, it is possible to produce a contour map of the surface of the optic (Figure 3).

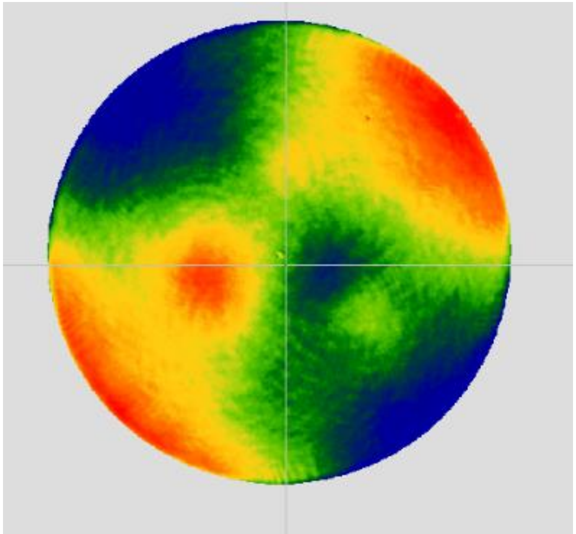

Figure 3: Surface of a spherical mirror (16.6 nanometre RMS) produced from the 4D PhaseCam.

The Surface map (Figure 3) displays the flatness of the surface; red being the elevated regions and blue representing the depressed regions. Interferograms are vital as they allow one to visualise a surface to extremely low measurements. In the contour map (Figure 3), the most elevated region is only 200 nanometres above the zero plane, demonstrating the possible precision of interferometer technology.

1.3 Origins of interferometry

The first idea for an interferometer came in 1867 from French physicist Armand Hippolyte Louis Fizeau **[3]**. Fizeau proposed that the resolution of telescopes could be improved if the light signals received could be combined via constructive interference. However, due to the available technology at the time he was unable to construct an instrument that was capable of combining light waves as they emerged from a telescope. It wasn't until 1891 where Albert Abraham Michelson constructed the first working interferometer. He made use of this new invention by attempting to determine the diameter of Jupiter's satellites, in which he was successful. In 1887 Michelson's interferometer technology was involved in arguably the most famous "failed" experiment to date - the Michelson-Morley experiment. The unsuccessful experiment was conducted in an attempt to detect the relative motion of matter through the stationary luminiferous ether. This changed the foundations of physics and led to Albert Einstein's theory of relativity. This experiment has been referred to as the moving-off point for the theoretical aspects of the Second Scientific Revolution **[4]**. Over the next 60 years interferometry has been an integral part of numerous scientific breakthroughs, predominantly in the field of astronomy. Various new designs for interferometers were invented including the Twyman-Green, Mach-Zehnder and Sagnac interferometers. In 1946, British radio astronomer Martin Ryle, working alongside Derek D. Vonberg built the first interferometer that could operate in the domain of radio waves. This led to numerous new celestial objects being discovered.

1.4 Aberration Theory & Zernike Polynomials

Understanding aberrations is vital in optical metrology as its principal purpose is to determine the aberrations present in an optical component or an optical system **[5]**. The two types of Wavefront aberrations are monochromatic (Seidel and wave) and chromatic (Longitudinal, Transverse) aberrations. Chromatic aberration is a type of distortion in which there is a failure of a lens to focus all colours to the same convergence point. This occurs because lens's have different refractive indices for different wavelengths of light. With regards to monochromatic aberrations, there are five primary types of Seidel aberrations, these being Spherical aberration, Coma, Astigmatism, Field curvature and Distortion each with their own unique properties (Figure 4).

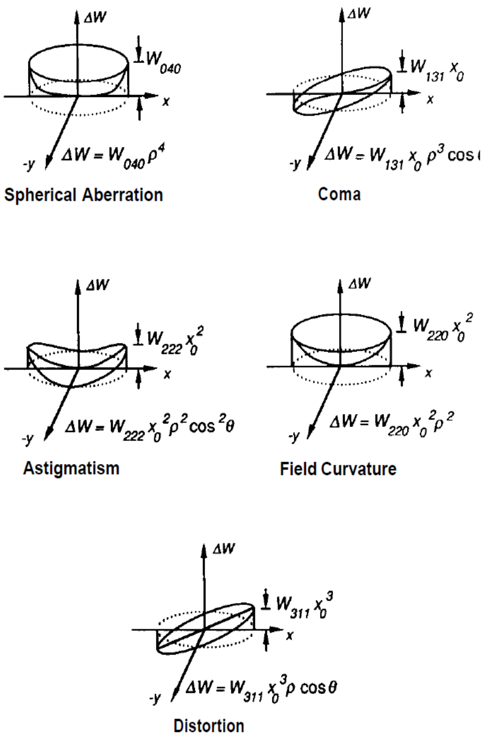

Figure 4: Seidel Aberrations. **[5]**

Zernike polynomials are the standard way of modelling aberrations of a surface **[5]**. They are a complete set of orthogonal polynomials across the unit circle, and with the use of coefficients the polynomials can be used to describe the surface of almost any optical part.

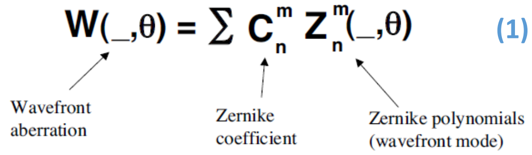

(1)

Equation (1) displays how a Wavefront is represented by a sum of Zernike polynomials, each with its own coefficient. Although Zernike polynomials are primarily used for spherical surfaces they can be adjusted to work for a range of different shaped optical surfaces. However, this method has proved to be far inferior. There are an infinite amount of Zernike polynomials, but almost any spherical surface can be accurately represented with the use of around 120 of these polynomials. There are also different orders of Zernike polynomials, each being orthogonal to every other. A few of these polynomials are shown in Figures 5 & 6.

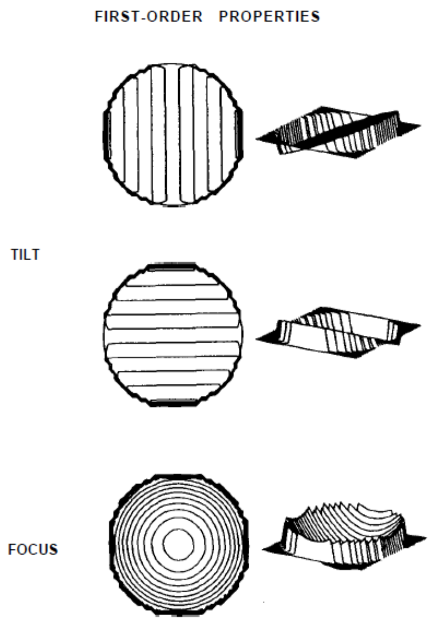

Figure 5: Examples of First order Zernike Polynomials. **[5]**

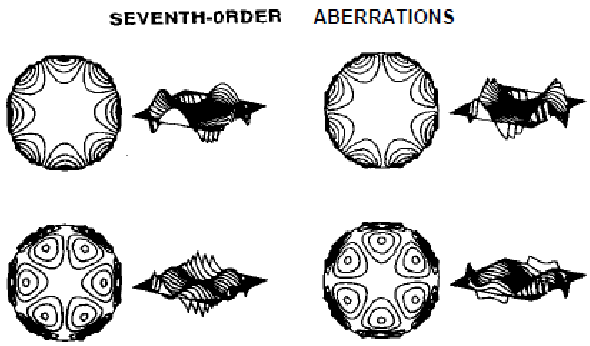

Figure 6: Examples of Seventh-order Zernike Polynomials. **[5]**

2.1 The 4D Technology "dynamic" PhaseCam 6000 laser interferometer

The 4D PhaseCam interferometer uses proprietary, high speed, high resolution wave front sensors to measure the shape of optical surfaces to extreme accuracy. This equipment is an extremely impressive piece of technology and is currently being implemented at a number of high precision optical metrology facilities. The 4D PhaseCam is phase shifting interferometer based on the Twyman-Green design (Figure 7).

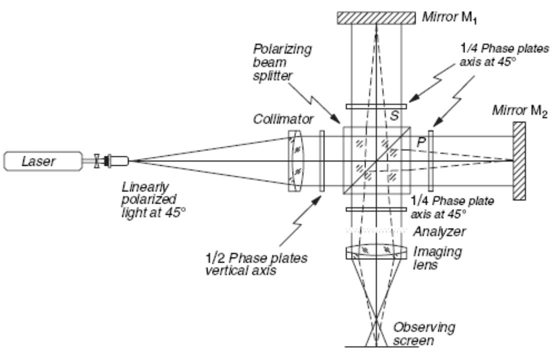

Figure 7: Phase shifted Twyman-Green interferometer. **[6]**

Accompanying the 4D PhaseCam is an advanced piece of software, 4Sight. The 4D PhaseCam along with the software allows one to view the surface of an optic in real time, eliminating the need to manually analyse the interferograms. 4Sight has many features, such as the ability to remove certain aberrations that could be attributed to the test set up itself rather than from the optic under testing. It also provides over 120 Zernike coefficients for different polynomials used to map the surface of the optic. The aforementioned features makes the 4D PhaseCam interferometer one of the industry's leading technologies. But as mentioned, the 4D PhaseCam interferometer is expensive thus eliminating the majority of the market. The 4D PhaseCam also comes with a limited amount of keys to access 4Sight. The purchase of additional keys is extremely expensive and cause a problem for operations with smaller budgets.

2.2 Promising interferometer technology

For an interferometer to be successful in the industry it must be accurate, affordable, have a efficient software package and be user friendly. Promising designs includes the Twyman-Green, Mach-Zehnder and Bath interferometers. Each of these are simple in design and inexpensive to construct by comparison.

2.3 Twyman-Green Interferometer

Created in 1916 by Frank Twyman and Arthur Green, the Twyman–Green interferometer is a variant of the Michelson Interferometer and although primarily used to test optical components, it has applications in other fields such as optometry research **[7]**. As depicted in Figure 8, the design of a basic Twyman–Green interferometer is extremely simple, allowing for the possibility to replace components with little trouble, in turn should lowering the cost of the product. This technology can be designed to have an interferometric resolution of up to 30 nanometres **[8]**. Although this value of exceptionally accuracy, it still falls short of the 4D PhaseCam interferometer in terms of potential accuracy, thus eliminating this technology from consideration.

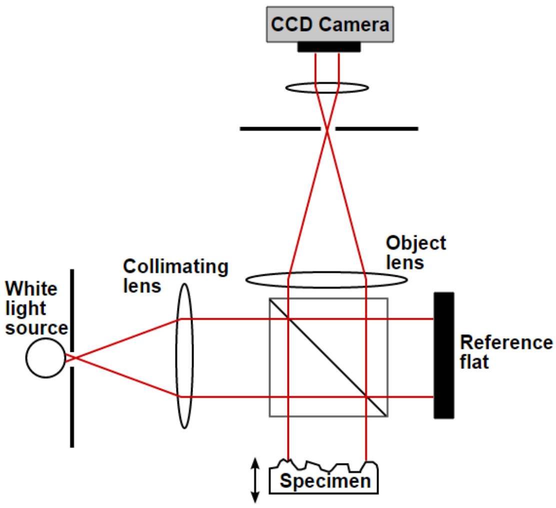

Figure 8: Twyman-Green interferometer. Credit: Wikimedia

2.4 Mach-Zehnder Interferometer

The Mach-Zehnder interferometer is named after Ludwig Mach and Ludwig Zehnder whom concocted the idea in the early 1890s. This design is widely used in today's technology and frequently used in the fields of plasma physics, aerodynamics **[9][10]**, astronomy **[11]**, quantum dynamics **[12]** and optics **[13]**. This design is widely used as it allows one to measure both reflective and refractive surfaces.

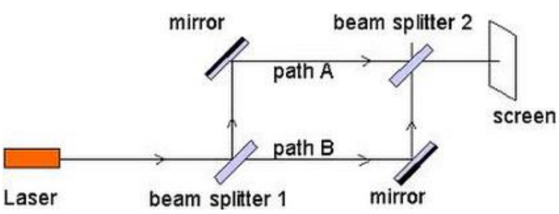

Figure 9: Mach–Zehnder interferometer. Credit: Wikimedia

A Mach-Zehnder interferometer is highly configurable and adaptable, but unlike the Twyman-Green and Michelson interferometers, each of the light paths is only traversed once. Although this design can be utilised to measure surfaces, it is far more effective at measuring transparent samples/gases by placing the sample container along one of the paths of light **[14]**. As the Mach-Zehnder interferometer was primarily designed to measure transparent samples its accuracy when dealing with reflective surfaces significantly drops. The size of the apparatus is also significantly large as there are many components to the device and therefore could become problematic when designing one that is easy to operate. All the aforementioned points will be too problematic to overcome and therefore this design must be removed from consideration.

2.5 Bath Interferometer

The last and most promising of the possible designs is that of the Bath interferometer. With its compact, highly adjustable and versatile design, it is the ideal candidate for an affordable/accurate interferometer. The Bath interferometer was invented by Karl-Ludwg Bath in the early 1970s and is derived from the Gates interferometer described in Malacara's book Physical Optics & Light Measurement **[15]**. Karl-Ludwg Bath published a paper on his invention in 1973 **[16]**. Although this technology has been around for over 40 years, it is only since the previous half-decade that this design is being truly considered as a precise interferometer. Its design is extremely simple and only requires a few components to operate (Figure 10). With the use of a light source (laser), beam splitter, small mirror and a lens an interference pattern can be created representing the surface of the optic.

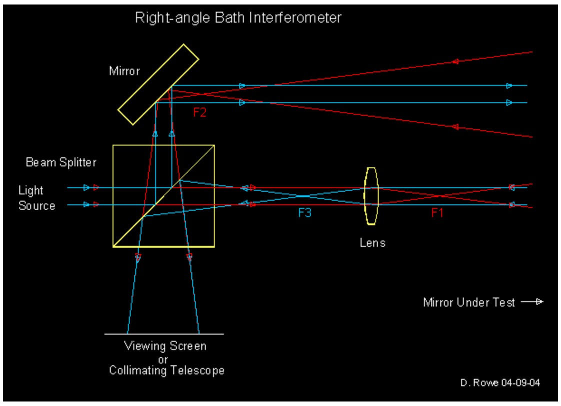

Figure 10: Bath interferometer. Credit MediaWIki

Figure 10 depicts a right-angle version of the Bath interferometer. A collimated light source is divided by the beam splitter into the (blue) reference beam and the (red) test beam. The reference beam hits the mirror under test, reflects from this surface, passes through the lens and comes to a focus at F3. As for the test beam, it is expanded into a spherical wave by the lens, which has a focus at F1. The expanding beam illuminates the mirror being tested and comes back to focus at F2. The two expanding beams pass back through the beam splitter and interfere at the detector.

Due to its simple design, questions have been asked of its potential accuracy. After searching for papers on Bath interferometers, it arose that very few papers have been published on this technology. However, after further research, a few non peer reviewed papers emerged. Although there legitimacy can be questioned, they can provide a better insight into Bath interferometers. Michael S. Scherman wrote a report in 2012 discussing potential of the Bath interferometer **[17]**. Although the results produced are extremely promising, there is no direct comparison to the readings produced from any other interferometer, providing little certainty in the results. Although mentioned, there is also no analysis of environmental effects such as vibrations and thermal air currents, proving no insight into how these factors affect the readings. There have been a few papers comparing different interferometers, but none involving a Bath interferometer. This is likely due to interest in the Bath interferometer recently emerging. A report by Stephen C. Koehler provided a comparison between 3 different interferometers **[18]**. Koehler achieved this by comparing the surface maps of individual readings, averaged readings and Zernike coefficient values. Koehler report provides a great insight into how interferometer comparison should be conducted, but once again, environmental effects were not tested causing potential discrepancies with accuracy.

The Bath interferometers design allows the interferometer to be extremely compact and also allows components to be exchanged easily. This is vital, as measuring different size optics requires diverging lenses of different focal powers. As considered, the design of the Bath interferometer allows for the lens to be swapped effortlessly. There are also free analysis software programs available online in the form of OpenFringe and FringeXP. These two software's can read the fringe patterns of the interferograms and provide a contour map of the surface along with the coefficients for the Zernike polynomials.

Measurement astigmatism is inherent in the Bath interferometer due to the lateral separations of the beams. Although this astigmatism is usually small enough to be tolerated, correction is required to obtain the most accurate results. Although this correction tool is a built in function in the aforementioned software's, the path-length difference (OPD) attributed to astigmatism is given by Equation (2).

$$OPD = \frac{D^2 d^2}{16R^3} \quad (2)$$

D is the diameter of the mirror under test, d is the beam to beam separation, R is the radius of curvature of the mirror and OPD is the optical path difference the longest and shortest paths to the mirror.

3 Future research

The Bath interferometer appears to be the ideal candidate due to its versatility, simplicity and accuracy. Once constructed, the prototype Bath interferometer will undergo vigorous testing of its capabilities, such as its susceptibility to environmental factors (which has not been conducted before), its alignment procedure, the importance of the quality of each component (thus learning if it's possible to purchase cheaper components to lower production cost) and most importantly how the measurements from different size optics compare with the 4D PhaseCam. This information will lead to a conclusion of whether or not this technology should be streamlined and be commercially distributed.

4 Citations

[1] Kim, Sug-Whan; Walker, David ; Brooks, David. (2003). **Active profiling and polishing for efficient control of material removal from large precision surfaces with moderate asphericity**. *Mechatronics*. 13 (1), 295-312.

[2] Eso News. (2014). ***Another world-first for scientists in telescope race***. Available: http://www.glyndwr.ac.uk/en/AboutGlyndwrUniversity/Newsandmediacentre/Newsarchive/PressReleases2014/ESOnews/. Last accessed 02.12.2014.

[3] **H**ellemans, Alexander; Bryan Bunch (1988). ***The Timetables of Science***. New York City: Simon and Schuster. 317.

[4] Earl R. Hoover (1977). ***Cradle of Greatness: National and World Achievements of Ohio's Western Reserve***. Cleveland: Shaker Savings Association. 20.

[5] Wyant, James C. (1992). **Basic Wavefront Aberration Theory for Optical Metrology. In: Wyant, James C.** ***APPLIED OPTICS AND OPTICAL ENGINEERING, VOL. XI***. Arizona: Academic Press, Inc. 1-53.

[6] Malacara, Daniel. (2007). **Polarizing Cube Beam Splitter**. In: Malacara, Daniel *Optical Shop Testing*. 3rd ed. New York: A John Wiley & Sons, Inc.. 46-70.

[7] Tomasz J. Licznerski ; Henryk T. Kasprzak ; Waldemar Kowalik. (1999). **Application of Twyman–Green Interferometer for Evaluation of In Vivo Breakup Characteristic of the Human Tear Film**. *J. Biomed. Opt*. 4 (1), 176-182.

[8] Podbielska, Halina Ewa. (1996). **High precision Twyman-Green interferometer for the measurement of ophthalmic surfaces**. *Acta Ophthalmologica Scandinavica*. 74 (4), 348-353.

[9] Goldstein, R J. (1965). **Interferometer for Aerodynamic and Heat Transfer Measurements**. *AIP*. 36 (1), 1408.

[10] Ristić, Slavica. (2012). **Flow visualization techniques in wind tunnels – optical methods (Part II)**. *Military Technical Institute*. 1 (1), 38-49.

[11] Dohlen, K.. (2004). **Phase masks in astronomy: From the Mach-Zehnder interferometer to coronagraphs**. *EAS Publications Series*. 12 (1), 33-44.

[12] Gerry, Christopher C. (1999). **Generation of optical macroscopic quantum superposition states via state reduction with a Mach-Zehnder interferometer containing a Kerr medium.** *Phys. Rev*. 59 (1), 40-95.

[13] Heideman, R.G. ; Lambeck, P.V.. (1999). **Remote opto-chemical sensing with extreme sensitivity: design, fabrication and performance of a pigtailed integrated optical phase-modulated Mach–Zehnder interferometer system**. *Sensors and Actuators B: Chemical*. 61 (1-3), 100-127.

[14] Min Xiao ; Yong-qing Li ; Shao-zheng Jin ; Julio Gea-Banacloche. (1995). **Measurement of Dispersive Properties of Electromagnetically Induced Transparency in Rubidium Atoms**. *Phys. Rev*. 74 (1), 666.

[15] Malacara, Daniel (1989). ***Physical Optics and Light Measurements***. New York: Academic Press . 43- 150.

[16] BATH, Karl-Ludwig. (1973). **A simple interferometer for testing astronomical optics** . *Sterne und Weltraum*. 6 (1), 177-180.

[17] Scherman, Michael S. (2012). **Laser Interferometry of Parabolic Newtonian Telescope Mirrors with a Bath Interferometer and Analysis of Wavefront and Figure in OpenFringe.** Unpublished work.

[18] Koehler, Stephen C. (2005). **Interferometry Comparison**. Unpublished work.